Geomorphology 402 (2022) 108130

Contents lists available at ScienceDirect

Geomorphology

journal homepage: www.journals.elsevier.com/geomorphology

Tectonic controls on geomorphology and spatial distribution of monogenetic volcanoes in the Central Southern Volcanic Zone of the Andes (Argentina)

Fernanda S. Santos [a,*], Carlos A. Sommer [a], Maurício B. Haag [a,b], Walter A. Báez [c], Alberto T. Caselli [d,e], Alejandro D. Báez [d,e]

[a] Instituto de Geociências, Universidade Federal do Rio Grande do Sul, Av. Bento Gonçalves 9500, Porto Alegre, RS, Brazil
[b] Department of Earth Sciences, University of Toronto, 22 Ursula Franklin Street, Toronto, ON M5S 3B1, Canada
[c] IBIGEO (Universidad Nacional de Salta - CONICET), Av. Bolivia 5150, Salta, Provincia de Salta, Argentina
[d] Universidad Nacional de Río Negro, Instituto de Investigación en Paleobiología y Geología, Río Negro, Argentina
[e] Consejo Nacional de Investigaciones Científicas y Técnicas (CONICET), Instituto de Investigación en Paleobiología y Geología, Río Negro, Argentina

ARTICLE INFO

Keywords:
Monogenetic volcanism
Geomorphology
Southern Volcanic Zone
Andes
Spatial Analysis
Geographic Information System

ABSTRACT

Monogenetic volcanoes are among the most common volcanic landforms on Earth. The morphology and distribution of small volcanoes can provide important information about eruption dynamics and tectonics. The Southern Volcanic Zone of the Andes (CSVZ) comprises one of the most active magmatic regions on Earth. Characterized by the presence of polygenetic volcanoes and calderas in a complex tectonic setting, this region also hosts hundreds of small, back-arc monogenetic volcanoes. In this contribution, we apply a Geographic Information System (GIS) that combines imagery data and digital elevation models to establish the first comprehensive dataset of monogenetic volcanoes in the CSVZ (38° to 40° S), exploring their eruption dynamics and relationship to tectonic and structural processes. Combining spatial analysis and geomorphological observations, we identify the presence of 335 monogenetic volcanoes distributed into nine clusters, now grouped in the Zapala Volcanic Field (ZVF). The ZVF is marked by the predominance of cinder cones (80%) followed by phreatomagmatic volcanoes (20%), suggesting some influence of external water in the eruption dynamics. Generally, monogenetic vents present a clear association with local and regional lineaments, suggesting a strong structural control on the occurrence of the monogenetic deposits in the ZVF. The higher vent densities are observed in the southern Loncopué Though, an important extensional feature related to tearing of the subducted Nazca plate underneath the South American Plate. Morphometric parameters of cinder cones indicate variable stress orientations in the CSVZ that possibly results from the oblique tectonics in the region. From north to south, the maximum principal stress rotates from NE-SW to E-W and becomes progressively less constrained as it distances from the current magmatic arc. Based on the relative ages, we map the evolution of monogenetic volcanism through time. Our results suggest a waning in the monogenetic activity in ZVF over time. When compared to monogenetic fields in the Central Andes, the ZVF is marked by higher vent densities and number phreatomagmatic landforms, with the absence of lava domes. This ultimately reflects the contrasting crustal structure and climate conditions of these two regions.

1. Introduction

Small monogenetic volcanoes are among the most common volcanic landforms on Earth (Wood, 1979), and they can occur as isolated vents, grouped in volcanic fields, and as parasitic vents associated with polygenetic systems (Fornaciai et al., 2012; Kereszturi and Németh, 2012a; Uslular et al., 2015). These landforms are generally classified according to edifice morphology, which depends on endogenous (e.g., magma composition and volatile content) and exogenous (e.g., structural context, interaction with surface water, terrain slope, and wind intensity) factors (Kereszturi and Németh, 2012a; Kervyn et al., 2012; Di Traglia et al., 2014; Németh and Kereszturi, 2015). Because of these

* Corresponding author.
E-mail address: 00316383@ufrgs.br (F.S. Santos).

https://doi.org/10.1016/j.geomorph.2022.108130
Received 22 July 2021; Received in revised form 20 January 2022; Accepted 25 January 2022
Available online 31 January 2022

controls, several eruption styles are associated with monogenetic volcanoes, including hawaiian, strombolian, and hydrovolcanic (Kereszturi and Németh, 2012b; Németh and Kereszturi, 2015; Báez et al., 2017).

The morphology of monogenetic volcanoes and their spatial distribution reflect important parameters about the dynamic of the volcanic field and their tectonic controls (e.g., structural control and emplacement dynamics; Bemis and Ferencz, 2017). Several studies have shown that edifice morphology and spatial distribution can be used to identify relevant volcanological and tectonic processes, including eruption dynamics, structural and tectonic settings (Tibaldi, 1995; Kereszturi and Németh, 2012a; Haag et al., 2019; Marliyani et al., 2020). In recent years the availability of high-resolution Digital Elevation Models (DEMs) and satellite imagery fostered the remote characterization of monogenetic volcanoes. This approach yielded interesting results, allowing a deeper understanding of volcanology, structural, and tectonic processes related to monogenetic volcanic fields (e.g., Bruno et al., 2006; Kiyosugi et al., 2012; Németh and Kereszturi, 2015; Haag et al., 2019; Morfulis et al., 2020; Uslular et al., 2021).

The central segment of the Southern Volcanic Zone of the Andes (CSVZ) comprises one of the most active magmatic regions on Earth (Stern, 2004). In addition to the presence of polygenetic volcanoes and calderas (e.g., Copahue in Argentina, Callaqui, Antuco, and Llaima in Chile), this region also hosts hundreds of small back-arc monogenetic volcanoes (Fig. 1). Despite their widespread presence in the area, only a few studies have addressed the occurrence of monogenetic volcanism in the CSVZ (e.g., Muñoz and Stern, 1989; Lara et al., 2006; Cembrano and Lara, 2009) and none of them deals with the geomorphology of these volcanoes.

In this contribution, we use a GIS to report the first complete catalog of monogenetic landforms in CSVZ (henceforth grouped in the Zapala Volcanic Field - ZVF), their morphology, spatial distribution, and structural relationships. Combining satellite imagery and DEMs, we map and classify the monogenetic volcanoes in the region, establishing their eruption dynamics and relationship to tectonic features and processes.

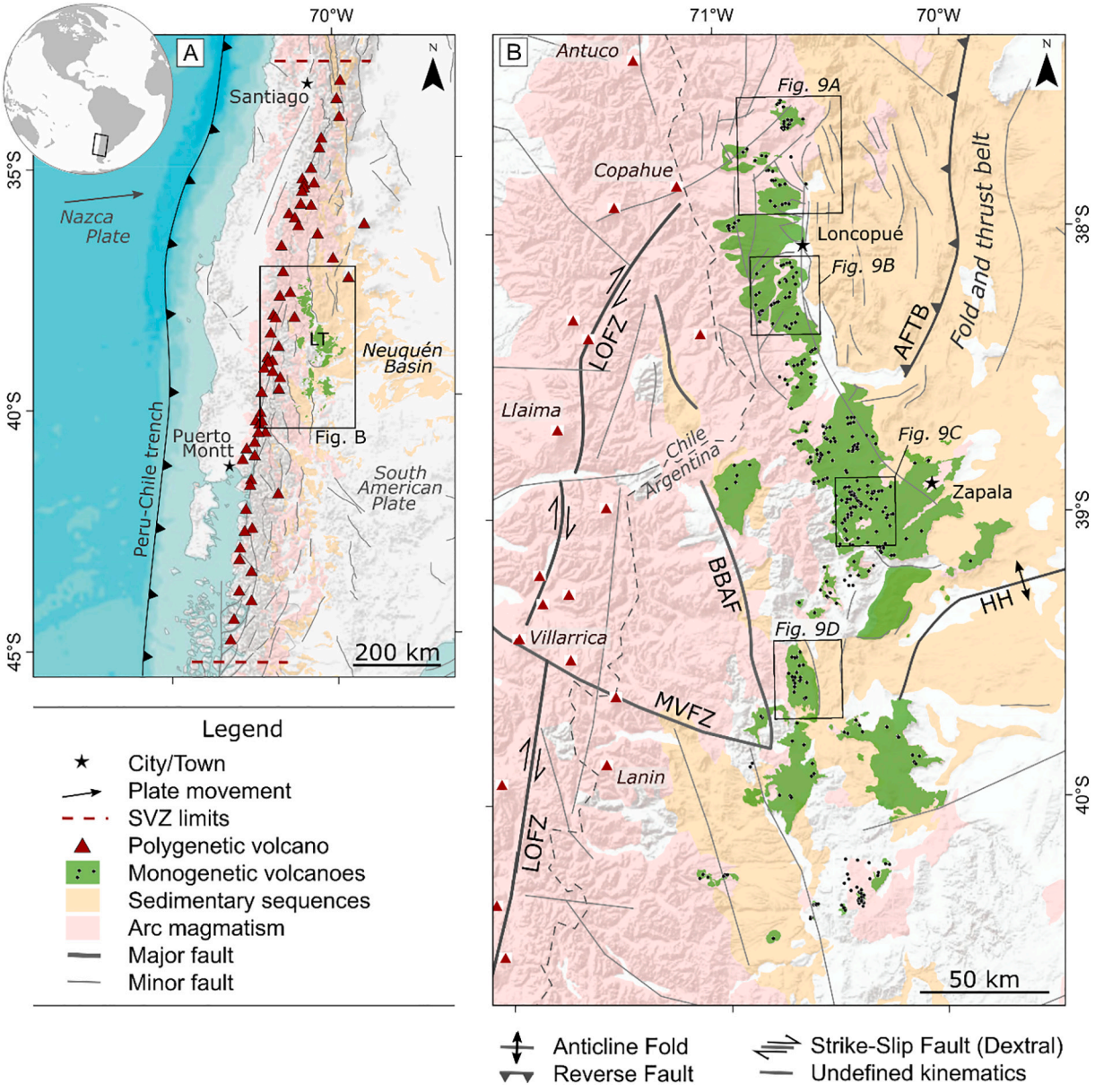

Fig. 1. A) Regional context of the studied area in the Andean Belt; B) regional map of the CSVZ with ZVF deposits, polygenetic volcanoes, and the main structural features. LT - Loncopué Trough. Structures are: AFTB - Agrio Fold and Thrust Belt, BBAF - Bío-Bío Fault Zone, HH - Huincul High, LOFZ - Liquiñe-Ofqui Fault Zone, MVFZ - Mocha-Villarica Fault Zone. Geological units after Cordani et al. (2016).

2. Geological setting

The CSVZ is located in the southern segment of the Andes and extends between latitudes 37° to 41°5′ S, involving regions of Argentina and Chile (Fig. 1). It is part of one of the four volcanic segments associated with the active convergent margin, located on the west coast of South America, where the Cocos, Nazca, and Antarctic plates are subducted by the South American plate (Hickey-Vargas et al., 2002) responsible for the Andean orogeny in the last 200 Ma (e.g., Mpodozis and Ramos, 2008). The CSVZ features hundreds of monogenetic back-arc volcanoes with extensive deposits and variable morphologies, in addition to the presence of numerous large polygenetic systems, such as composite volcanoes and calderas.

The eastern foothills of the Andes between the 31° and 40° S are defined by a significant retroarc basin that comprises a Late Triassic-Early Cenozoic succession called Neuquén Basin (Howell et al., 2005; Fig. 1A). The complex evolution of this basin can be divided into three main phases: (1) the opening of the basin in Late Triassic times, as a result of extensional processes that generated a series of long, narrow depocenters filled with volcanic/volcaniclastic and continental deposits (Vergani et al., 1995; Franzese and Spalletti, 2001; Howell et al., 2005; Carbone et al., 2011), (2) a post-rift phase of thermal subsidence during the Early Jurassic, when an active subduction regime and the magmatic arc are established on the western margin of Gondwana (Franzese et al., 2003; Howell et al., 2005; Mpodozis and Ramos, 2008), and (3) a phase of typical foreland basin between the Late Cretaceous and Early Cenozoic, resulting from the development of a compressive tectonic regime that generated the eastward migration of the orogenic front (Franzese et al., 2003; Howell et al., 2005; Tunik et al., 2010; Gianni et al., 2018).

The magmatic activity retreated toward the west in the Oligocene-early Miocene and a series of extensional basins (e.g., Cura Mallín basin) are generated in the foothills of the Neuquén Andes (Radic et al., 2002; Morabito Garcia and Folguera, 2005; Ramos and Folguera, 2005). The second period of deformation of the Neuquén Basin and a new expansion of the magmatism to the foreland is produced during the Middle-Late Miocene (Ramos and Folguera, 2005; Kay et al., 2006). The magmatic front begins to retreat again during the early Pliocene, associated with intense volcanic activity and the opening of the Cola de Zorro Basin in the Main Andes between the 37° and 39°S (Vergara and Muñoz, 1982; Muñoz and Stern, 1988; Folguera et al., 2006; Ramos and Folguera, 2005).

The Pliocene-Quaternary volcanism in the Neuquén region is mainly developed in an N-S belt parallel to the Andean front and the Tromen and Auca Mahuida volcanic fields located further east (Fig. 1B; Folguera et al., 2011). Particularly, a relevant Pliocene-Quaternary activity is focused on the Loncopué Trough (Fig. 1B). This is a narrow, N-S topographic depression of 200 km in length located between the 36°30′ and 39°S and limited by the Agrio fold and thrust belt to the east and the volcanic arc to the west (Folguera et al., 2010; Rojas Vera et al., 2010, 2014; Folguera et al., 2011; Pesce et al., 2019). The basal volcano-sedimentary infill of the axial part of the depression starts in the early Pliocene (Cola de Zorro Formation), followed by silicic distal pyroclastic sequences associated with the development of a series of calderas in the west during Pleistocene times, and the posterior emplacement of a basaltic cover in the western sector (Rojas Vera et al., 2014; Pesce et al., 2019).

Finally, significant Pleistocene-Holocene monogenetic basaltic fields develop in the Loncopué Trough, even extending to the Laguna Blanca/Zapala area (~39°S) (Groeber, 1928; Varekamp et al., 2010; Folguera et al., 2011; Rojas Vera et al., 2014). These flows consist of olivine-rich basalts that have received different names based on their relative age and location (e.g., Hueyeltué, Huechahue, Malleo, Macho Viejo, Los Mellizos, and Laguna Blanca basalts) (Leanza et al., 1997; Zannettini et al., 2010). Varekamp et al. (2010) analyzed the volcanic centers south of the 37°30′S, including those located around the Laguna Blanca/Zapala area (~39°S), and observed transitional chemical features between intraplate and arc magmas. However, the centers located in the northern sector of the Loncopué Trough show typical arc signatures (Rojas Vera et al., 2014).

3. Methods

3.1. Landform identification, mapping a classification

Monogenetic volcanoes consist of small-volume, nearly circular to elliptical, landforms with either positive (cinder cones, tuff cone, and lava domes) or negative topography (maars - phreatomagmatic structures) (Lesti et al., 2008; Kereszturi and Németh, 2012a; Németh and Kereszturi, 2015; Smith and Németh, 2017; Haag et al., 2019). Based on these criteria, we identified possible monogenetic volcanoes in the study area using Google Earth® (1 to 10 m/px) to establish a primary dataset (Fig. 2A). In this step, we also rely on the available geological maps that contain the distribution of eruptive products of monogenetic volcanism (i.e., lava flows) for some regions in the study area (Kay et al., 2006; Melnick and Echtler, 2006; Cembrano and Lara, 2009; Varekamp et al., 2010; Rojas Vera et al., 2014; Pesce et al., 2019, 2020).

This preliminary dataset was then verified using satellite imagery in ArcMap®. In this process, the landforms were classified into the following categories: cinder cone, maar, tuff ring, tuff cone, and lava dome (Fig. 2A), following the categories proposed by Kereszturi and Németh (2012a) and Németh and Kereszturi (2015). Using this approach, we find out that monogenetic volcanoes in the study area are either cinder cones or maars. To characterize these volcanoes and perform the geomorphological measurements, we used a high-resolution (12.5 m/px) DEM derived from the ALOS PALSAR sensor, which provides full coverage of the studied area and can be freely downloaded at the Alaska Satellite Facility website (available at https://vertex.daac.asf.alaska.edu/). To ensure consistency the DEM was set to an equal-area projection (UTM 19S).

From the DEM we used ArcMap® 10.5 to derive several terrain attributes, including slope, contour, and aspect (Fig. 2B), which are useful for mapping the monogenetic volcanoes. Based on these maps and satellite images, we performed a supervised (i.e., manual) geomorphological mapping of the volcanoes and their associated deposits (at a local scale of 1:10,000, Fig. 2C to the left). Based on the mapping and the contour plots, we performed an ellipse fitting and the morphometric measurements using ArcMap Spatial Analyst (Fig. 2C, to the center).

For cinder cones, we measured the maximum basal width (W_M), minimum basal width (Wm), the height of the cone (Hc), and maximum flank slope (Sco) (Fig. 2C). For maar volcanoes, we measured the depth of the crater (Dc), as well as the maximum (D_M) and minimum crater diameter (Dm) (Fig. 2C). We also take the azimuth of the maximum diameter W_M and D_M, which is better explained in Section 3.3. *Morpho-structural analysis*.

3.2. Spatial analysis

The spatial analysis allows the identification of the degree of clustering, the detection of subclusters, and the internal organization of the monogenetic vents. After mapping and classification of the targets, point analyzes were performed using the spatial analysis tools in ArcMap® applying the methodology proposed by Bishop (2007).

The identification of the number of monogenetic clusters in ZVF was based on the methods of Cañón- Tapia (2016), using kernel density functions. According to the search radius, the number of detected clusters follows a power-law distribution in which the inflection point indicates the optimum number of clusters within a monogenetic field (Cañón- Tapia, 2016; Morfulis et al., 2020).

The distribution pattern within each monogenetic cluster was analyzed using the Average Nearest Neighbor (ANN) analysis (Bruno, 2004). In this method, the *observed* distance among monogenetic vents (Ro) in a given area (A_{HULL}) is compared to the *expected* distance of

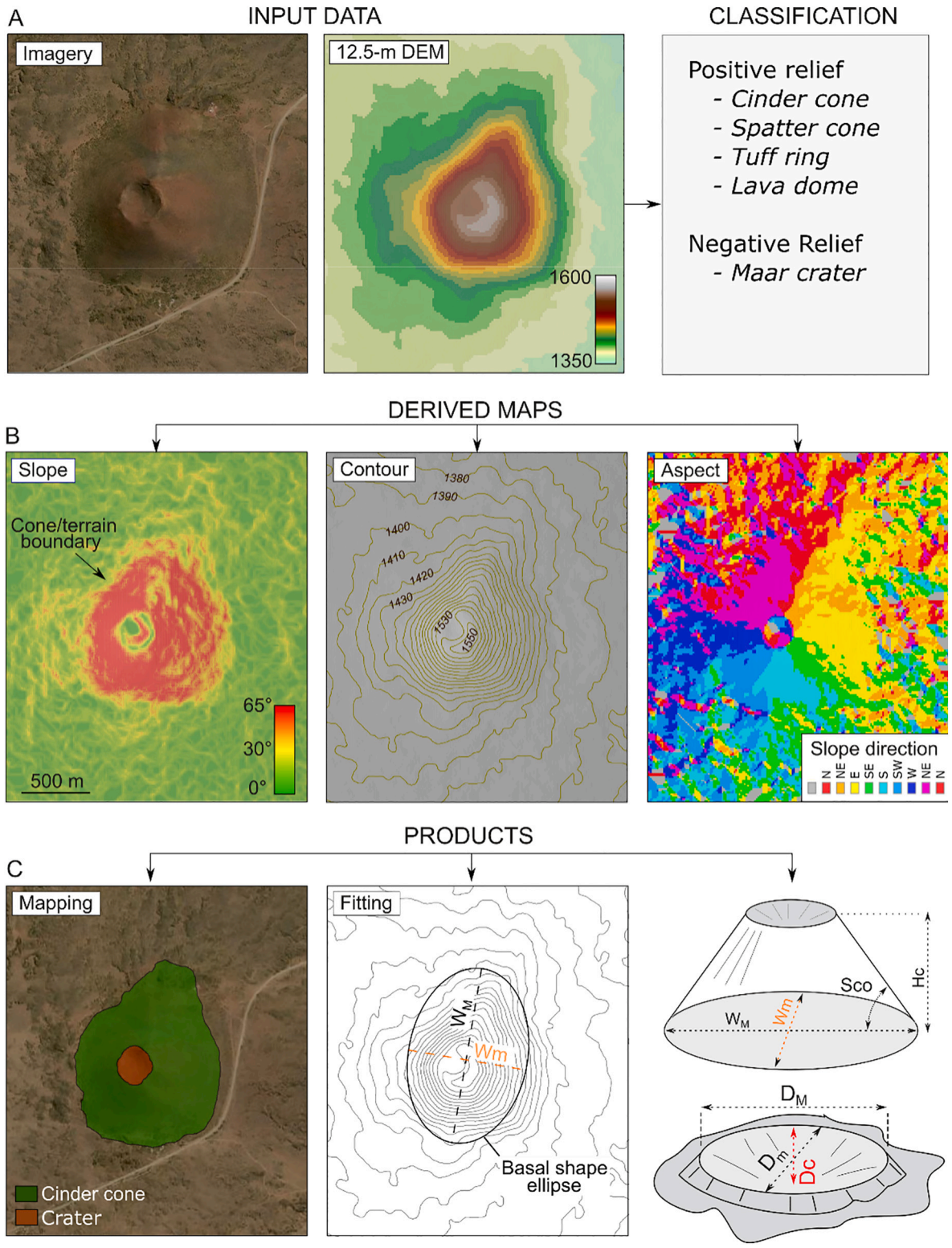

Fig. 2. The methodology applied to this study: A) imagery and DEM (elevation scale in meters) comprise input data, which were used to identify and classify the monogenetic landforms; B) DEM-derived maps include slope (scale in degrees), contour (10-m interval curves) and aspects (slope direction); C) supervised (manual) mapping, ellipse fitting and measurements of the monogenetic landforms. Abbreviations are W_M - Cone maximum basal width; W_m - Cone minimum basal width; Hc - cone heigh; Sco - cone flank slope; Dc - maar crater depth; D_M - maximum diameter of maar crater; D_m - minimum diameter of maar crater.

evenly distributed vents (Re). The R-statistic parameter results from the Ro/Re ratio and indicates whether the points distribution follows a Poisson (R-statistic = 1), clustered (R-statistic → 0.0), or dispersed (R-statistic → 2.0) distribution (Bishop, 2007).

3.3. Morpho-structural analysis

The determination of stress state can be inferred from the spatial distribution of monogenetic vents and their main attributes (Fig. 3;

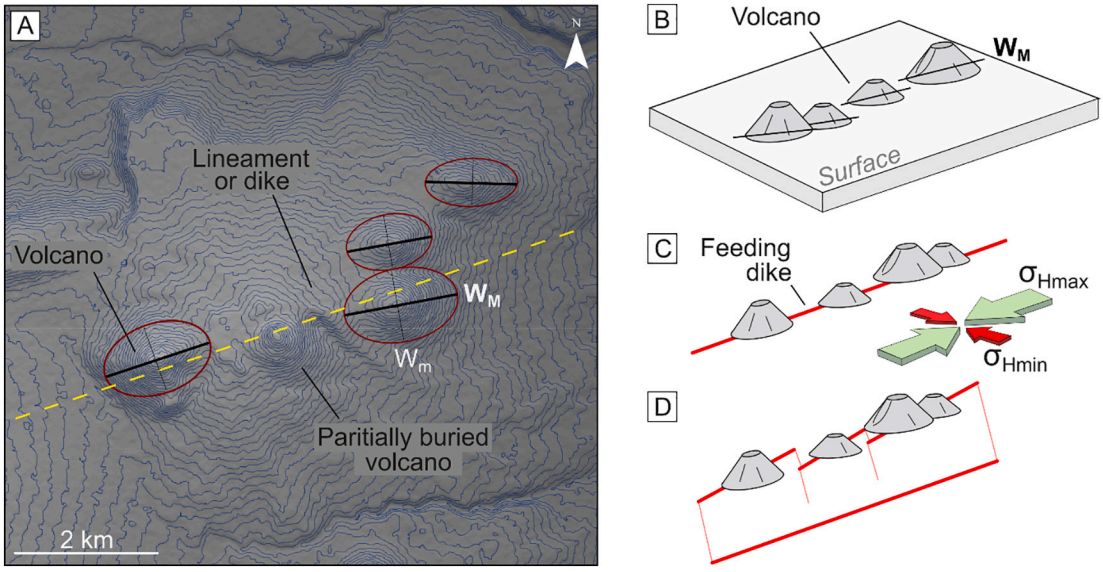

Fig. 3. Morpho-structural and lineament analysis. A) Hillshade image with contours used for ellipse fitting and measurement of W_M and Wm for cones or D_M and Dm for maars - cone heigh; B) sketch of the surface expression of monogenetic cones; C) subsurface sketch of inferred plumbing system based on cone basal elongation for normal faulting; D) subsurface sketch of the inferred plumbing system for strike-slip and *en echelon* geometries; σHmax - maximum horizontal stress; σHmin - minimum horizontal stress.

Tibaldi, 1995; Paulsen and Wilson, 2010; Bonali et al., 2011; Le Corvec et al., 2013; Tadini et al., 2014; Haag et al., 2019; Marliyani et al., 2020; Morfulis et al., 2020). In this context, the surface distribution of monogenetic volcanoes and their elongation (Fig. 3A, B; Tibaldi, 1995) can be used to infer the orientation of subsurface structures, such as dike, fractures, and faults, which ultimately reflect the local stress state (Fig. 3C, D).

To determine the relationship between monogenetic vents and the structural setting in the ZVF we followed a similar approach to Tibaldi (1995) and Bonali et al. (2011), using morphometrics to infer the states of stress.

To this end, we measure directional parameters for each monogenetic volcano using ellipses (Fig. 3A) and measuring the basal elongation of cones (azimuth of W_M) and crater elongation of maars (azimuth of D_M). We also calculate the ellipticity for both cones and maars by dividing the minimum for the maximum diameter of these features (W_m/ W_M; Tibaldi, 1995). In the case of cinder cones, we did not measure crater elongation and crater-rim depressed points (e.g., Tibaldi, 1995) because these features are either absent or not completely clear in most of the studied cones in the ZVF.

Finally, we also measured alignments of both cinder cones and maars. Vent alignment/dike presence was determined using at least three vents, and by observing the presence of elongated cones (W_m/ W_M < 0.8) or dikes (Fig. 3A), following the recommendations of Le Corvec et al. (2013) and Paulsen and Wilson (2010). In this study, we did not use densities plots to infer conduit and dike orientations (e.g., Cebriá et al., 2011; Tadini et al., 2014) because it generally neglects morphometric and field evidence that result in more robust results (Paulsen and Wilson, 2010).

Both vent alignment and the basal elongation of monogenetic volcanoes/maar craters are parallel to the maximum horizontal stress (σHmax) and perpendicular to the minimum horizontal stress (σHmin), as suggested by several studies (Fig. 3C; e.g., Nakamura, 1977; Tibaldi, 1995; Lara et al., 2006; Haag et al., 2019; Marliyani et al., 2020). Monogenetic cones may also be slightly oblique to the main feeding system, suggesting an *en echelon* distribution (Fig. 3D). In the structural analysis, we only consider cones emplaced in flat surfaces (slope $< 5°$) and without significant modification (i.e., extensively degraded cones and maar craters).

3.4. Relative age

In monogenetic fields, the number and distribution of active volcanoes can vary over time (Le Corvec et al., 2013). Differently from other regions in the Andes that have extensive well-dated ignimbrite deposits and abundant radiometric ages, thus allowing a better constraint on the spatial evolution of the magmatism (e.g., the Central Andes, Tibaldi et al., 2017), the volcanoes in the ZVF do not have this database yet.

As an alternative to determining the spatio-temporal evolution of monogenetic volcanism in the ZVF, we assigned relative ages to the cinder cones based on morphometric attributes including crater, cone, and lava flow integrity. These attributes reflect modification stages to the original, conical shape of cinder cones and are mainly based on simulation and geomorphological observations (Hooper and Sheridan, 1998; Fornaciai et al., 2012; Kereszturi and Németh, 2012b; Zarazúa-Carbajal and De la Cruz-Reyna, 2020).

Following this approach, cinder cones were grouped into four categories (Fig. 4), following an adaptation of the methods of Haag et al. (2019): young - cinder cones with well-defined craters and basal limits, smooth surfaces, and absence of erosional features; moderately young - cones without a well-defined crater and roughly defined basal limits, with deep and well-established gullies and rills; mature - cones without a well-defined crater and roughly defined basal limits, with ravines and rills; old - reduced landforms, without a defined crater basal limit, cut by deep ravines and rills. Using this classification method, we created regional maps of relative age in the studied area, comparing our results with the available absolute ages from the literature (e.g., Ramos and Folguera, 2005).

4. Results

4.1. Geomorphology and morphometry

We identify 335 monogenetic volcanoes in the study area, with a predominance of cinder cones (80%) followed by phreatomagmatic (maars) volcanoes (20%). Monogenetic deposits (volcanoes and their associated lava flows) cover approximately 6.400 km^2 in the CSVZ. The main morphological attributes are represented in Fig. 5, while the

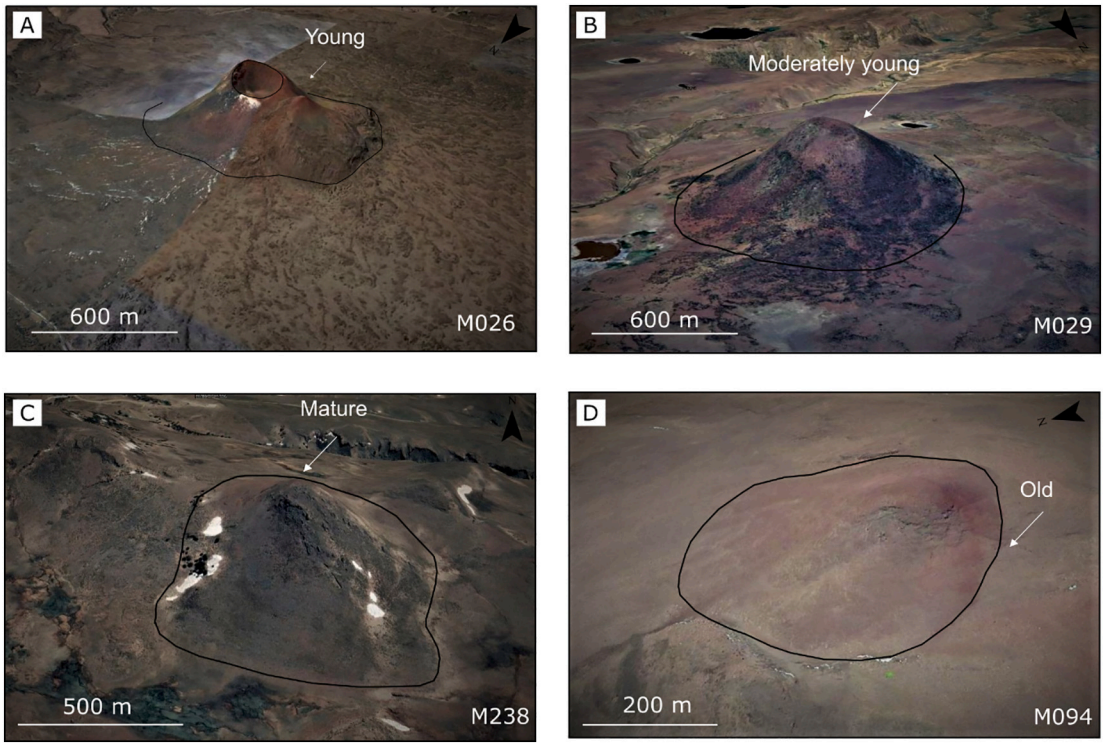

Fig. 4. Relative age classes of studied cinder cones. A) young (coordinates are 39° 01′ 22.76″ S; 70° 22′ 28.88″ W); B) moderately young (38° 58′ 37.84″ S; 70° 24′ 31.40″ W); C) mature (38° 53′ 30.92″ S; 70° 33′ 43.71″ W); D) old (37° 59′ 20.14″ S; 70° 56′ 31.35″ W). Relative scale due to perspective. Vertical exaggeration of 3. Source: GoogleEarth (2021).

distribution of monogenetic volcanoes and their main morphometric parameters are reported in Fig. 6A. All elevations are reported in meters above sea level (a.s.l).

4.1.1. Cinder cones

Cinder cones are the predominant landforms in the ZVF and exhibit a significant variation in their geomorphologic attributes (Fig. 5A, B, C). They are frequently breached, elongated edifices associated with extensive lava flows (Fig. 5A). In several cases, multiple generations of lava flows are observed, suggesting multiple eruptions in the same region (Fig. 5A). A few cinder cones occur nested inside maar craters that cut older lava flows (Fig. 5B). Several cones form clusters that can be grouped by lineaments and are possibly related to dikes and feeding systems (Fig. 5C).

Cinder cones occur throughout the entire study area (Fig. 6A, B), at terrain elevations ranging from 900 to 2200 m a.s.l. (Fig. 6B). They dominate the northern section (above ~ lat. 39°S) and higher terrain elevations (> 1600 m a.s.l.) (Fig. 6A, B, C). Below ~ lat. 39°S, the presence of maar volcanoes becomes more relevant (Fig. 6A, B, C).

The cinder cones also exhibit a significant variation in their morphometric parameters (Fig. 6E). Maximum basal widths (W_M) range from 246 to 3590 m and cone heights (Hc) from 7 to 426 m (Fig. 6E). Most cinder cones are generally elliptical, with W_m/W_M ratios ranging from 1.0 (circular) to 0.4 (highly elliptical) and clustering around 0.80 (Fig. 6E). Flank slope angles (Sco) from 6 to 40°. For a full report on the morphometric attributes please check Supplementary item 1.

4.1.2. Phreatomagmatic volcanoes: maar

Maar volcanoes are marked by well-preserved, generally circular craters, partially filled by alluvial sediments and saltpans (Fig. 5D, E, F). Crater limits are roughly delimited by small changes in elevations because ZVF maars often lack external tephra rings and deposits (Fig. 5D, E, F). Maar craters commonly cut lava plateaus (Fig. 5E) and are closely associated with cinder cones (Fig. 5F).

Maar volcanoes are preferentially present south of lat. 39° S (Fig. 6A, B) and at terrain elevations below 1600 m a.s.l (Fig. 6C). A summary of their main morphometric parameter is presented in Fig. 6F. The depth of the crater (Dc) ranges from 1 to 211 m, and the crater maximum axis (D_M) ranges from 142 m to 4900 m (Fig. 6F). Maar craters are often elliptical to nearly circular, with D_m/D_M ratios ranging from 0.99 (circular) to 0.39 (highly elliptical), while most D_m/D_M ratios are below 0.75 (Fig. 6F). For a full report on the morphometric attributes please refer to Supplementary item 1.

4.2. Spatial distribution

Spatial analysis was performed using Kernel density estimations for cluster identification and Average Nearest Neighbor (ANN) analysis for pattern determination.

4.2.1. Cluster identification

The identification of the number of the monogenetic clusters was based on the methods of Cañón- Tapia (2016). Following this method, we observe an inflection point at ~10 km (Fig. 7A; Cañón- Tapia, 2016; Morfulis et al., 2020). This value suggests a total of 9 monogenetic clusters (Fig. 7A, B) in the CSVZ. The vent density of each cluster is presented in Table 1. The maximum density of monogenetic volcanoes (0.144 vents/km^2) is located in cluster number 5 (Fig. 7B), about 30 km southwest of Zapala town (Fig. 7C), at the southern segment of the Loncopué Trough.

4.2.2. Distribution pattern

ANN analysis indicates a strong clustered pattern for ZVF, with an overall R-statistic of 0.392. A summary of ANN results is presented in Table 1. Individually, each monogenetic group presents variable distribution patterns, from clustered to dispersed (Fig. 8A, B). A clustered pattern is observable in groups 1, 5, and 9 (Fig. 8A), which present R-statistic ranging from 0.719 (less clustered) to 0.648 (most clustered), all

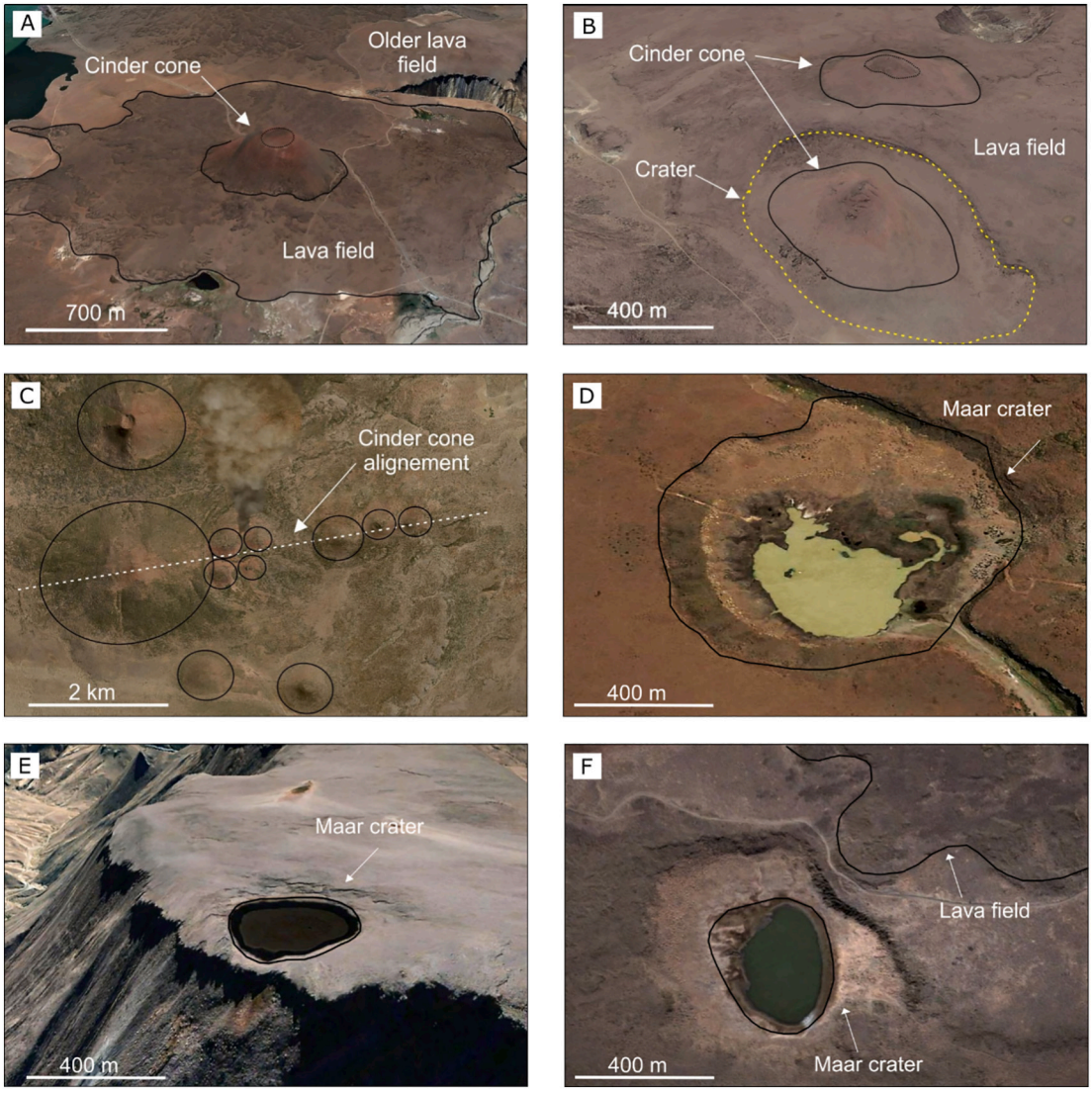

Fig. 5. Representative monogenetic landforms in the CSVZ: A) Cinder cone with associated lava flow (39° 05′ 32. 90″ S; 70° 23′ 16.80″ W); B) cinder cone emplaced inside a maar-crater (39° 09′ 18.90″ S; 30° 14′ 25.11″ W); C) composite alignment of multiple cinder cones (38° 55′ 59.42″ S; 70° 20′ 28.09″ W); D) maar crater emplace on top of thin volcanic sequences (39° 46′ 19.97″ S; 70° 22′ 54.39″ W); E) Maar crater emplace over volcano-sedimentary (39° 16′ 19.83″ S; 70° 33′ 42.16″ W); F) Maar craters associated with cinder cones (39° 35′ 47.31″ S; 70° 37′ 54.10″ W). Relative scale due to perspective. Vertical exaggeration of 3.
Source: GoogleEarth (2021).

well above the -2σ range (Fig. 8A, B). The dispersed pattern is recorded in groups 2, 4, 6, and 7, with R-statistic from 1.22 (less dispersed) to 2.30 (most dispersed). Groups 4 and 7 are above 1.65σ, while groups 2 and 6 are above 2.85σ (Fig. 8A, B). The Poisson pattern is detected only in groups 3 and 8 (Fig. 8A).

The spatial pattern and distribution of monogenetic volcanoes is better observed in detailed maps of each monogenetic group. Group 9 displays strongly clustered monogenetic vents (Fig. 8A). These vents form in sub-clusters inside the group perimeter (defined by the convex hull), in *E*-W trends to the southwest (inferred to be controlled by local structures), and isotropic groups to the north (Fig. 8C). In contrast, group 4 presents an opposite spatial pattern, with vents randomly dispersed inside the group area (Fig. 8D).

4.3. Structures and lineaments

Based on the satellite imagery and the available geological maps (e.g., Rojas Vera et al., 2014; Pesce et al., 2019), we map the occurrence of monogenetic centers in the study area and their relationship with structural features. A summary of the main structural settings observed in the ZVF is provided in Fig. 9. Structural data obtained from cone elongation and vent alignment indicate the predominance of *E*-W, ENE-WSW to WNW-ESE structures in the ZVF, with significant variations among the different clusters (Fig. 9).

Cluster 9 is the closest to the volcanic arc (~30 km considering the main trend of active polygenetic volcanoes) and is marked by monogenetic volcanoes mainly associated with E-W structures (Fig. 9A). The northern limit of cluster 9 is characterized by NE-SW alignments, next to the Trolón Caldera (Fig. 9A). Cluster 8 presents a slight change in vent alignment direction when compared to cluster 9, with most features trending EN*E*-WSW to WSW-ENE (Fig. 9B). Further south, cluster 5 is also marked by ENE-WSW to WSW-ENE trending vents (Fig. 9C). Several NW-SE trending monogenetic volcanoes are also present in the region (Fig. 9C). South of this region, the orientation of vents starts to become more scattered. Cluster 4 shows a variety of orientations, including ENE-WSW, WNW-ESE, NE-SW, and NE-SE trending volcanoes and alignments (Fig. 9D).

A summary of the quantitative structural data extracted from

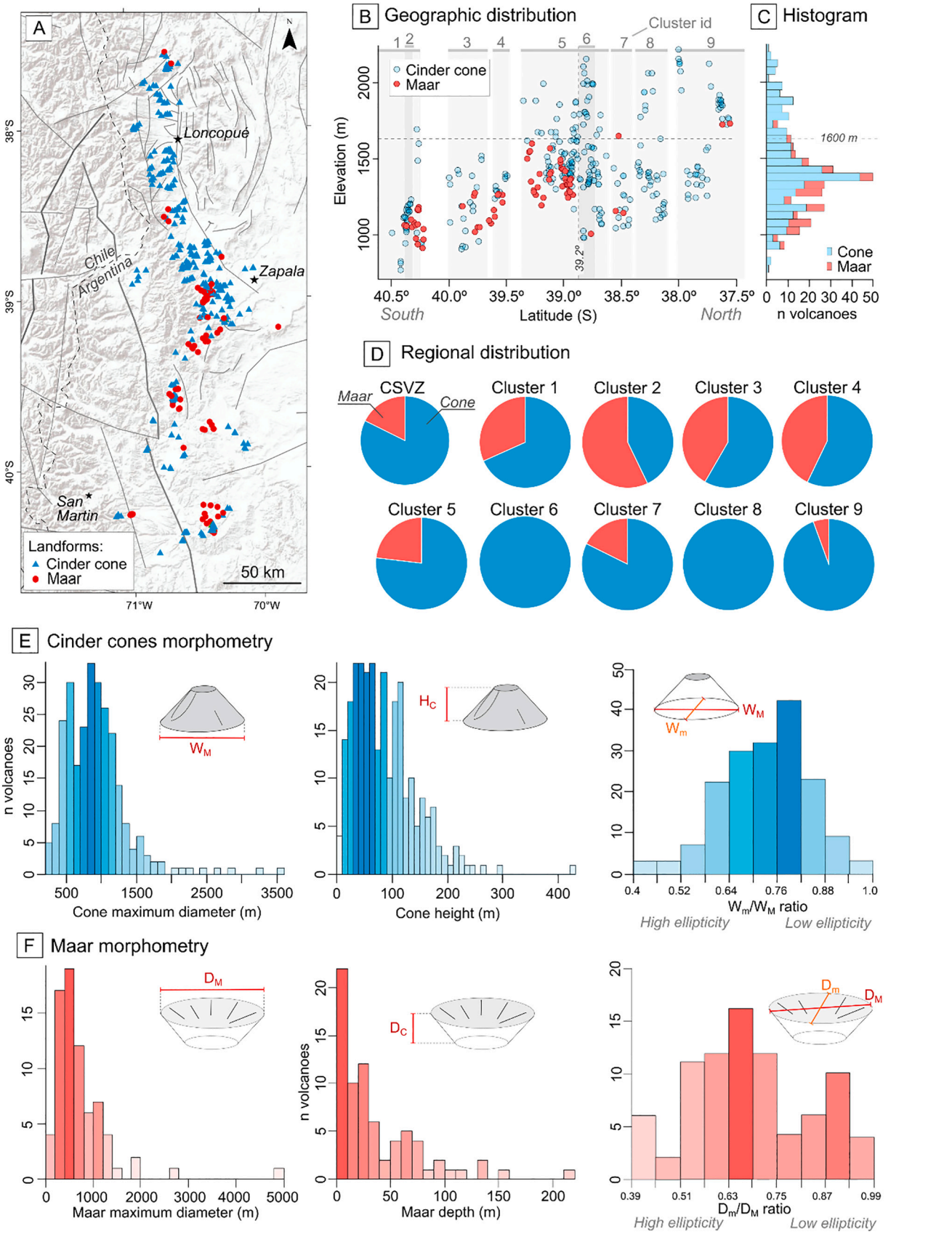

Fig. 6. Morphometric results. A) CSVZ map with the distribution of monogenetic landforms in the ZVF; B) North to the south geographic distribution of cinder cones and maars; C) histogram with the terrain elevation of cinder cones and maars; D) landform distribution of wet (represented by maars) and dry (represented by cinder cones) monogenetic landforms across the ZVF; E) Morphometric results (W_M, Hc, and ellipticity) for cinder cones; F) Morphometric results (D_C, D_M, and ellipticity) for maar volcanoes.

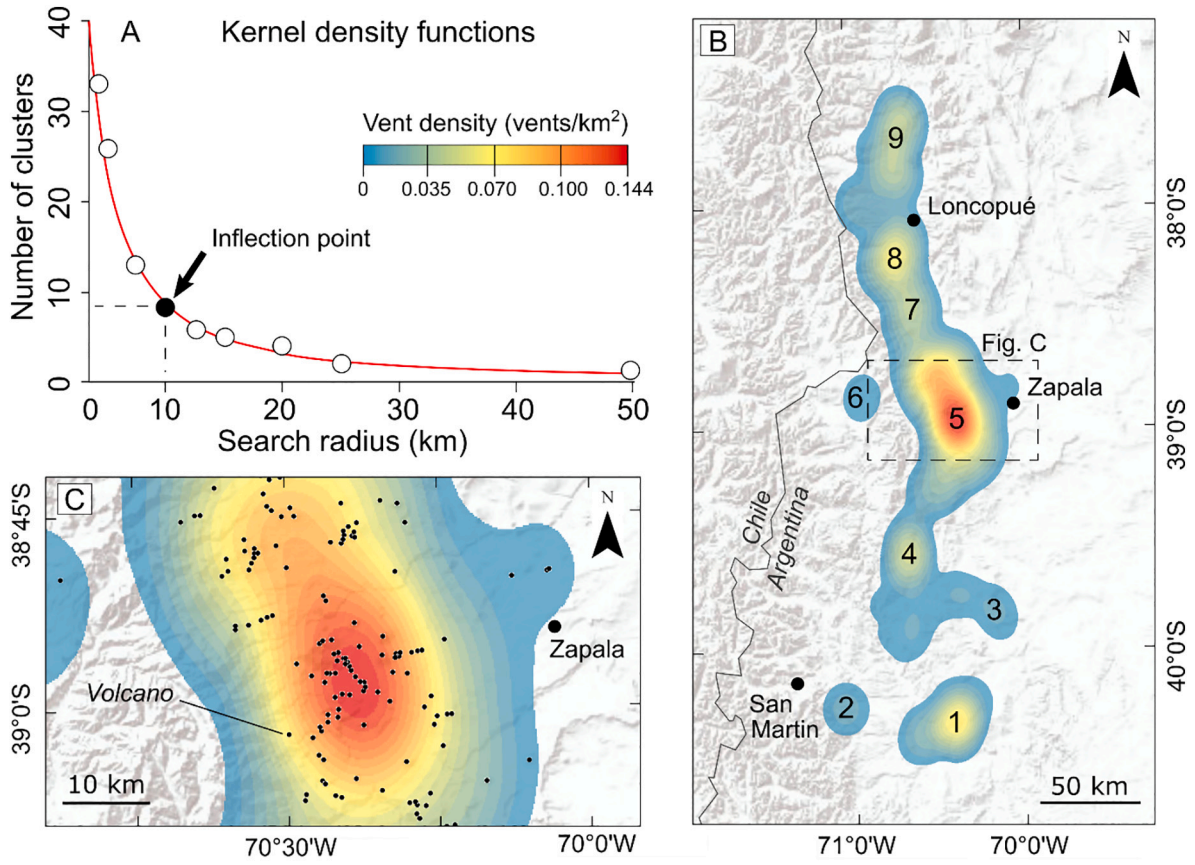

Fig. 7. Kernel density analysis. A) Number of kernel clusters as a function of the search radius; B) regional map with identified monogenetic clusters; C) detail map of cluster 5 showing the internal distribution of monogenetic vents in the southern Loncopué Trough.

Table 1
Spatial analysis results. ANN patterns are clustered (C), Poisson (P), and dispersed (D). A total of 20 vents comprise outliers that are not grouped in any given cluster.

Parameters	Entire ZVF	Cluster number								
		1	2	3	4	5	6	7	8	9
Vents	335	34	6	12	20	151	4	17	35	36
Area (km^2)	22.510	517	10	194	119	3.009	33	126	358	649
Average density (vent/km^2)	0.015	0.065	0.60	0.06	0.168	0.050	0.121	0.134	0.097	0.055
Maximum density (vent/km^2)	0.144	0.059	0.014	0.013	0.043	0.144	0.010	0.037	0.056	0.037
Re (m)	4932	2347	758	2343	1436	2564	1737	1700	1672	2519
Ro (m)	1938	1688	1276	2061	1746	1663	4010	2048	1668	1731
R-sta	0.392	0.719	1.683	0.879	1.21	0.648	2.307	1.222	0.997	0.687
Pattern	C	C	D	P	D	C	D	D	P	C

monogenetic volcanoes (cone and maar elongation, vent alignment, and dike orientation) is presented in Fig. 10. From north to south, there is an increase in the scattering of the basal cone orientation, as well as vent alignment (Fig. 10A). Despite this, histograms indicate a predominance of EN*E*-WSW elongated cones in the ZVF following azimuths ranging from 80 to 95° (Fig. 10B). This orientation is also confirmed by histograms of vent alignment and the orientation of dikes (Fig. 10C). If we consider the basal ellipticity values (W_m/W_M ratios) and exclude the nearly circular features (W_m/W_M ratios >0.8), it is interesting to note that we still obtain similar results, with higher kurtosis (i.e., more values close to the mean, Fig. 10D). Maar data indicate the presence of highly elliptical craters (low D_m/D_M ratios) mainly oriented along with ENE-WSW and WNW-ESE directions (Fig. 10E, F).

Rose diagrams built from these data allow better visualization of the orientation of monogenetic features in the ZVF (Fig. 10G). ENE-WSW to E-S directions prevail among the main orientations for basal cone elongation, vent alignment, and dike orientation (Fig. 10G). In contrast, the orientation of maar craters shows a higher dispersion when compared to cinder cones, with crater elongation ranging from ENE-WSW to WNW-ESE (Fig. 10G). These results contrast with the main lineaments observed in the fold and thrust belt region, which is marked by the predominance of N-S structures (Fig. 10G).

Deviations in basal cone orientation are also observed within each cluster (Fig. 10H). Clusters 1, 4, and 6 tend to show a more scatter pattern, while clusters 3, 5, 7, and 8 are marked by a predominance of E-W trending cones (Fig. 10H). Cluster 9 is the closest to the current volcanic arc (Fig. 9A) and presents a bimodal distribution of cinder cones basal elongation (Fig. 10H).

4.4. *Relative age*

Using the relative age classification method, it was possible to map

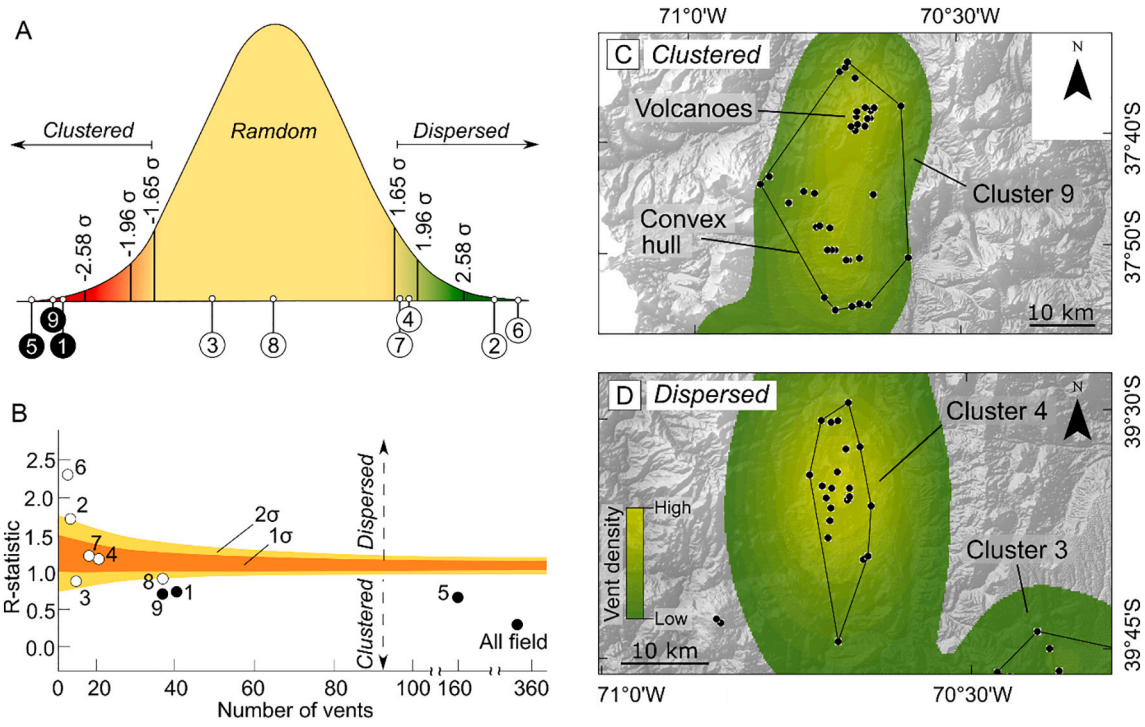

Fig. 8. Summary of ANN analysis. A) normal distribution with confidence intervals and the R-statistic for each monogenetic cluster; B) plot of R-statistic and number of vents; C) clustered pattern (R-statistic ~0.687), cluster number 9, and the respective convex hull area; D) dispersed pattern (R-statistic ~1.21), cluster number 4, and the respective convex hull area.

the temporal distribution of cinder cones in the ZVF. Similar to the approach used by Haag et al. (2019), we use relative ages of cinder cones to interpolate regional maps, expressing the results as density maps for each relative age class (Fig. 11A–D).

Our data indicate that the younger monogenetic volcanoes appear to concentrate southwest of Zapala Town (Fig. 11A), with more isolated occurrences a few kilometers northwest of Loncopué Town (Fig. 11A). Moderately young cones present a wide distribution to the eastward, apparently following an NW-SE-trending normal fault and concentrated in the Loncopué Though (Fig. 11B).

Mature landforms (moderately degraded landforms) are widespread in the study area and especially concentrate in the northwest and southwest regions of the Zapala and Loncopué Towns (Fig. 11C). These features present a similar distribution to moderately young landforms (Fig. 11B), however mature cones also occur as isolated clusters to the south of Zapala Town (Fig. 11C). Older monogenetic volcanoes are also widespread in the study area, with occurrences to the northwest of Loncopué, and next to the Chapuful volcano (Fig. 11D). Several old cinder cones also occur in the north-northwest of Zapala and the extreme southwest of the study region, near the city of San Martín along the Neuquén Basin (Fig. 11D).

5. Discussion

5.1. Geomorphology and morphometry

The monogenetic volcanism in the ZVF is marked by the predominance of cinder cones that present a clear association with local lineaments, suggesting a structural control on the occurrence of the monogenetic vents. The presence of cinder cones suggests a prevalence of the strombolian style as the main eruption dynamics in the ZVF (Németh and Kereszturi, 2015), similarly to the Puna Plateau in the Central Andes (Filipovich et al., 2019; Haag et al., 2019; Maro and Caffe, 2016; Morfulis et al., 2020). This dynamic is supported by the number of hydrovolcanic landforms in the region (less than 20%), which denotes a limited, however existing, influence of magma-water interaction through the eruption history of individual vents of the ZVF

The cinder cones present morphometric signatures (e.g., W_M, Hc) similar to extension-related cones when compared to the global dataset of Fornaciai et al. (2012) (Fig. 12A). These cones are marked by lower Hc/W_M ratios when compared to cinder cones associated with compressional environments (Fornaciai et al., 2012).

The use of traditional morphometric parameters (e.g., Hc/W_M ratio) to the determination of relative ages typically results in misleading interpretations (Hasenaka and Carmichael, 1985; Uslular et al., 2021), because morphometric parameters are subject to several post-emplacement modifications related to weathering and tectonics. Furthermore, many *syn*-eruptive processes can produce a variety of primary landforms, with extensive contrasts in Hc/W_M ratios (Kereszturi and Németh, 2012a, 2012b). In contrast, alternative approaches using cone flank slope (Sco) and contour curves have returned valid results (e.g., Inbar et al., 2011; Haag et al., 2019; Zarazúa-Carbajal and De la Cruz-Reyna, 2020). In ZVF cones, we observe a systematic decrease in Sco following the relative age, in which young landforms tend to present higher Sco values when compared to the older ones (Fig. 12B). Despite this general trend in average values, there is a considerable deviation and scattering in the data (Fig. 12B). This scattering is likely associated with contrasting initial cone morphology, which is mainly controlled by tectonics, terrain slope, and eruption dynamics (Kervyn et al., 2012; Bemis and Ferencz, 2017; Haag et al., 2019; Uslular et al., 2021).

Phreatomagmatic volcanoes tend to concentrate to the south of 39°S and typically below 1600 m a.s.l. (Fig. 6C), suggesting a geographic control on the occurrence of hydrovolcanism in the ZVF. This distribution may be associated with the decrease of water availability with increasing elevation. Using a global dataset of maar volcanoes, Sonder et al. (2018) observed a substantial decrease in the number of maar volcanoes above 2000 m a.s.l.

The sharp decrease in maar volcanoes observed in Fig. 6A and B may also be associated with geological controls. Phreatomagmatic activity depends on the availability, location, and proportion of groundwater

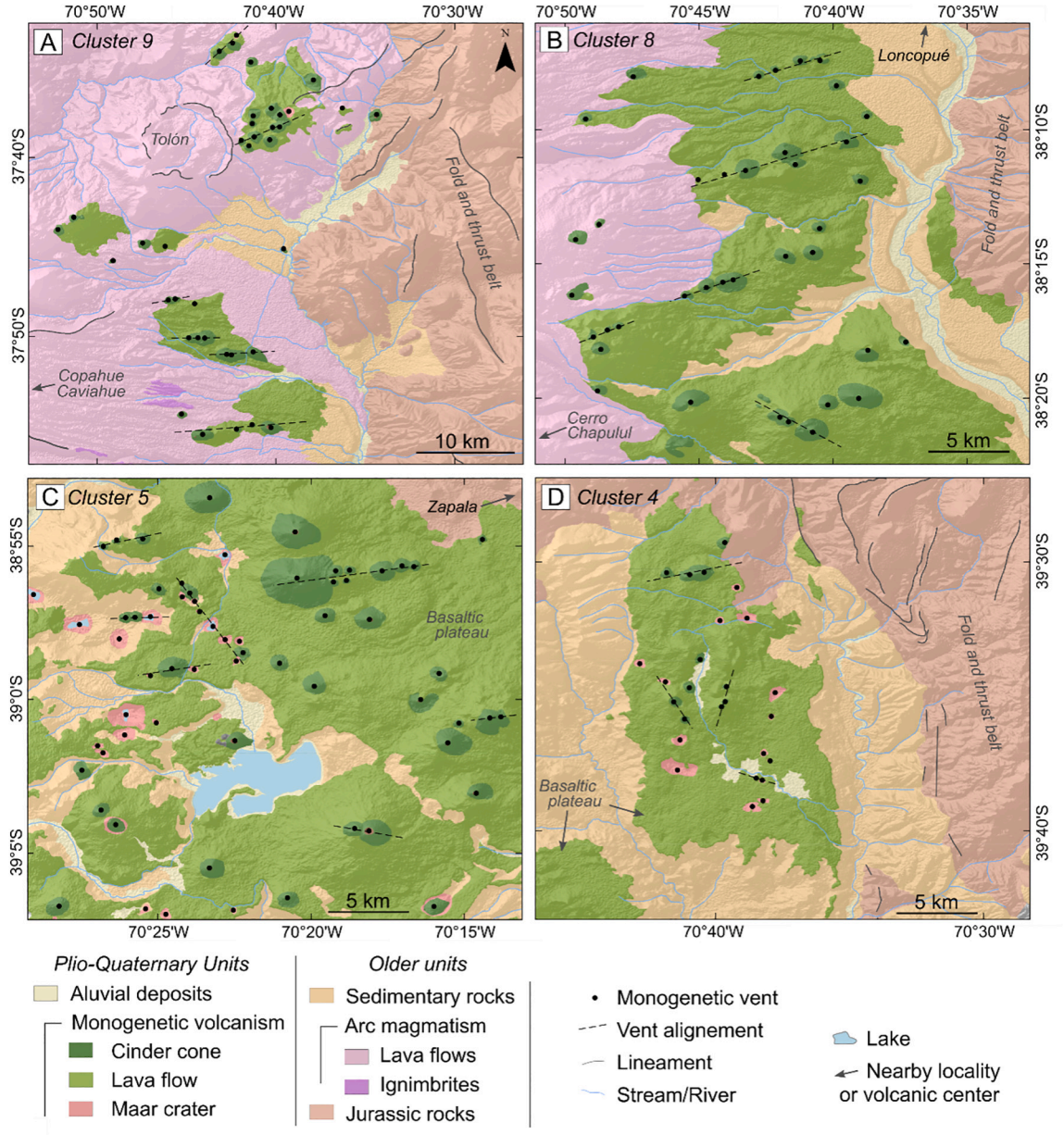

Fig. 9. Maps of monogenetic volcanoes in the ZVF and their structures, from north to south. A) cluster 9, with mainly E-W and subordinate NE-SW trending vents; B) cluster 8 with a predominance of NE-SW trending vents; C) southern section of Cluster 5, with E-W and NW-SE trending volcanoes; D) Cluster 4, with WSW-ENE, ENE-WSW, NNE-SSW, and NNW-SSE trending vents. Geological units based on Rojas Vera et al. (2014) and Pesce et al. (2019).

(Németh and Kereszturi, 2015; Ureta et al., 2021a). The regional basement to the south of 39°S is marked by the presence of sedimentary sequences of the Neuquén Basin, which possibly control the distribution of hydrovolcanism in the ZVF (D'Elia et al., 2016).

In contrast to cinder cones, the original morphology and subsequent modifications of maar craters are strongly controlled by substrate rheology. Ross et al. (2011) discuss these factors by comparing the morphology of maar craters emplaced on hard, soft, and mixed substrates in the Pali Aike Volcanic Field (Argentina). Mixed substrates are marked by the presence of soft (typically of sedimentary origin) and hard (typically volcanic or metamorphic) materials. Maar craters in the ZVF present variable depth/diameter ratios, suggesting a predominance of mixed substrates when compared to the dataset of Ross et al. (2011) (Fig. 12C). In the ZVF, maars with similar diameters but deeper craters are typically emplaced on top of sedimentary sequences capped by extensive lava flows, forming volcanic plateaus. In contrast, shallower maar craters are generally associated with soft substrates marked by sedimentary and alluvial sequences.

Additionally, several ZVF maars are proceeded by cinder cones, denoting a shift in the eruption dynamics from strombolian to phreatomagmatic. This dynamic behavior of phreatomagmatic eruptions/systems has been observed in several places around the world, including hyper-arid regions such as the Atacama Desert in Chile (Ureta et al., 2021a, 2021b). Ultimately, phreatomagmatic activity in these regions seems to be controlled by water availability and water table depth (Ureta et al., 2021b).

5.2. Spatial distribution

Monogenetic volcanoes in the ZVF present an average vent density of 0.015 vents/km^2. When compared to other monogenetic fields, the ZVF average density is higher than values obtained for the Southern Puna Plateau (0.008 vents/km^2; Haag et al., 2019), lower than the San Rafael (0.071 vents/km^2, in the USA; Kiyosugi et al., 2012), and significantly

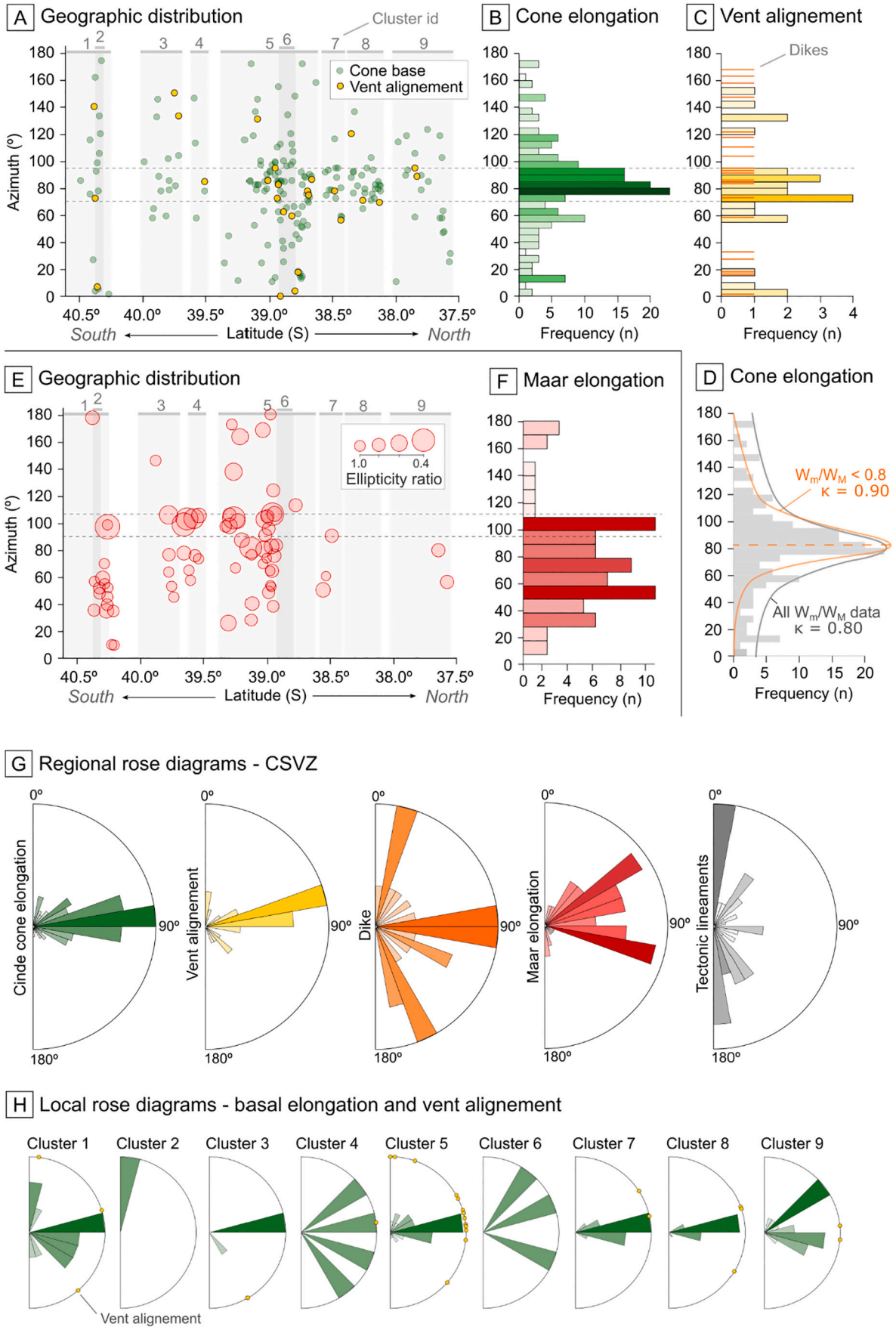

(caption on next page)

Fig. 10. Summary of structural analysis using monogenetic volcanoes: A) south to the north geographic distribution of cinder cones basal elongation and vent alignment; B) histogram of cinder cone elongation direction; C) histogram of vent alignment and dike direction, in orange; D) histogram of cinder cone elongation direction taking into account all cones and only the elliptical cones ($W_m/W_M < 0.8$), κ stands for kurtosis; E) south to the north geographic distribution of maar crater elongation; F) histogram of maar crater elongation direction; G) regional rose diagrams form cinder cone elongation, vent alignment, dikes, maar crater elongation, and the tectonic structures/lineaments; H) local rose diagrams of cinder cone elongation for each monogenetic cluster within the ZVF, vent alignment directions are represented as yellow dots.

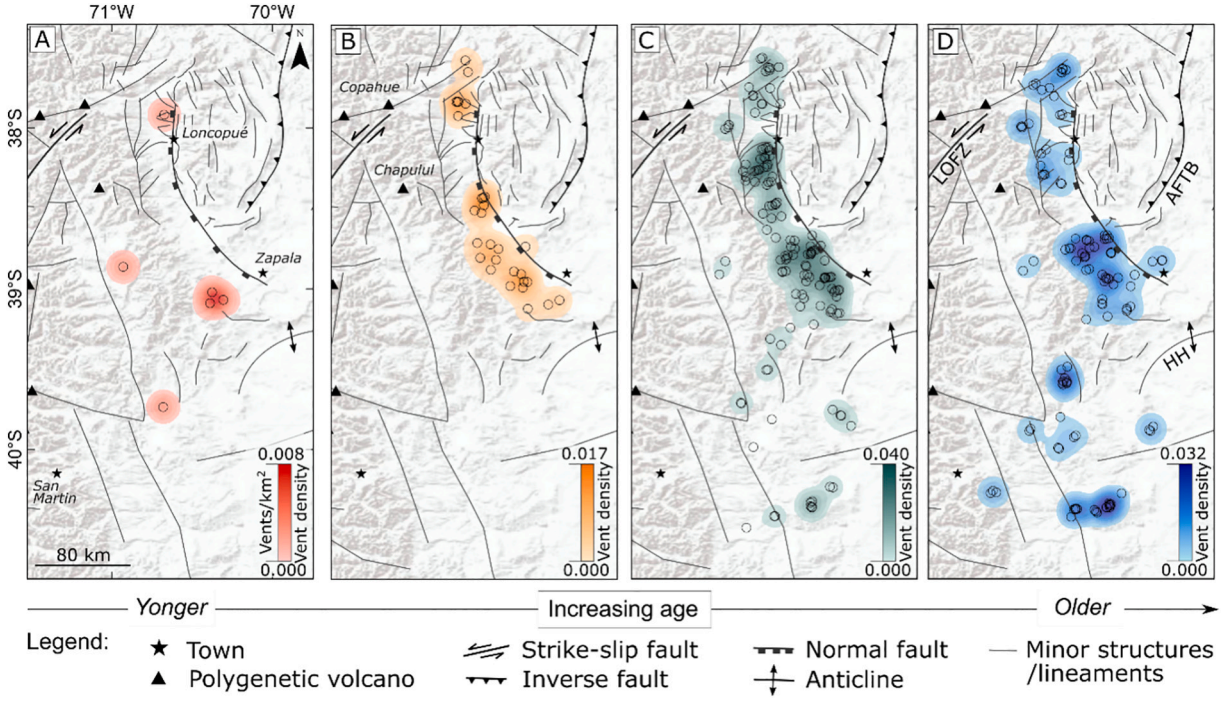

Fig. 11. Density maps with the regional distribution of each relative age class: A) young; B) moderately young; C) mature; D) old. Monogenetic volcanoes are expressed by open circles. All densities are in volcanoes/km^2.

lower than the Auckland (0.146 vents/km^2, in New Zealand; Le Corvec et al., 2013) and the Michoacán (0.260 vents/km^2, in México; Pérez-López et al., 2011) volcanic fields. In contrast, the ZVF maximum vent density of 0.144 vents/km^2 is comparable to values obtained for the Southern Puna (Haag et al., 2019; Morfulis et al., 2020). Similar to other monogenetic fields, the higher vent densities in ZVF are observed in the center of the monogenetic field, in cluster 5 (Fig. 7B).

The interplay of tectonics and magmatism controls the distribution of monogenetic volcanoes (e.g., Báez et al., 2017). The understanding of these dynamics and their surface expression has been the focus of several studies (e.g., Tibaldi, 1995; Tadini et al., 2014). Based on the distribution pattern of monogenetic vents in the Southern Puna Plateau, Morfulis et al. (2020) suggest two styles for monogenetic volcanic fields: (I) fields controlled by magmatic activity, with clustered pattern (R-statistic→ 0.0) and (II) field controlled by tectonics, with Random and Poisson distribution pattern (R-statistic→ 1.0).

The monogenetic vents in the ZVF present three distribution patterns: clustered (cluster 1, 5, and 9), Poisson distribution (clusters 3 and 8), and dispersed (cluster 2, 4, 6, and 7). This complex pattern is likely related to different magma production rates through the ZVF, where clusters 1, 5, and 9 would represent regions of relatively high and/or long-lasting magma supply (Báez et al., 2017; Morfulis et al., 2020).

5.3. Tectonic and structural implications

The Southern Andes is marked by a strong oblique component in the subduction of the Nazca Plate under the South American Plate (Fig. 1A; Stern, 2004). The oblique deformation in the Central SVZ is mainly accommodated by the 1200 km-long LOFZ (Cembrano et al., 1996), which controls the distribution of polygenetic volcanoes in the current volcanic arc. This setting offers a unique opportunity to examine the interplay of volcanic systems and tectonics. To date, the effects of this oblique tectonics on volcanism have been explored by a few studies, mainly focused on the orientation and morphology of stratovolcanoes located in the magmatic arc (e.g., Lara et al., 2006; Melnick and Echtler, 2006; Sielfeld et al., 2017).

Cembrano and Lara (2009) identify two sets of volcanic associations in the eastern (Chilean) SVZ based on volcano morphology and distribution: (1) NE-trending volcanoes that reflect the current tensional regime and (2) stratovolcanoes and monogenetic cones along the LOFZ that diverge in orientation with the current tensional regime. These observations, combined with structural data suggest an overall NE-SW trending maximum compressive stress (σ1) orientation at the magmatic arc (Fig. 13A; Cembrano and Lara, 2009 and references therein; Melnick and Echtler, 2006; Sielfeld et al., 2017). In contrast, studies about the morphology of monogenetic volcanoes and they relate to stress state in the back-arc SVZ are still scarce.

Based on edifice morphology and vent alignment, our data suggest that monogenetic vents in the CSVZ are preferentially emplaced along NE-SW and E-W trending structures (Fig. 10G). It is important to note that this result is consistent across different values of basal cones ellipticity, and even better constrained when considering only cones with ellipticity <0.8 (Fig. 10D). This suggests some common underlying control on the emplacement of the monogenetic cones in the study area. Therefore, this orientation can be used to infer the stress state (e.g., Le Corvec et al., 2013; Marliyani et al., 2020) in the CSVZ back-arc region, implying a maximum horizontal compressive stress (σHmax) with NE-SW to E-W direction, in agreement with Quaternary stress orientation

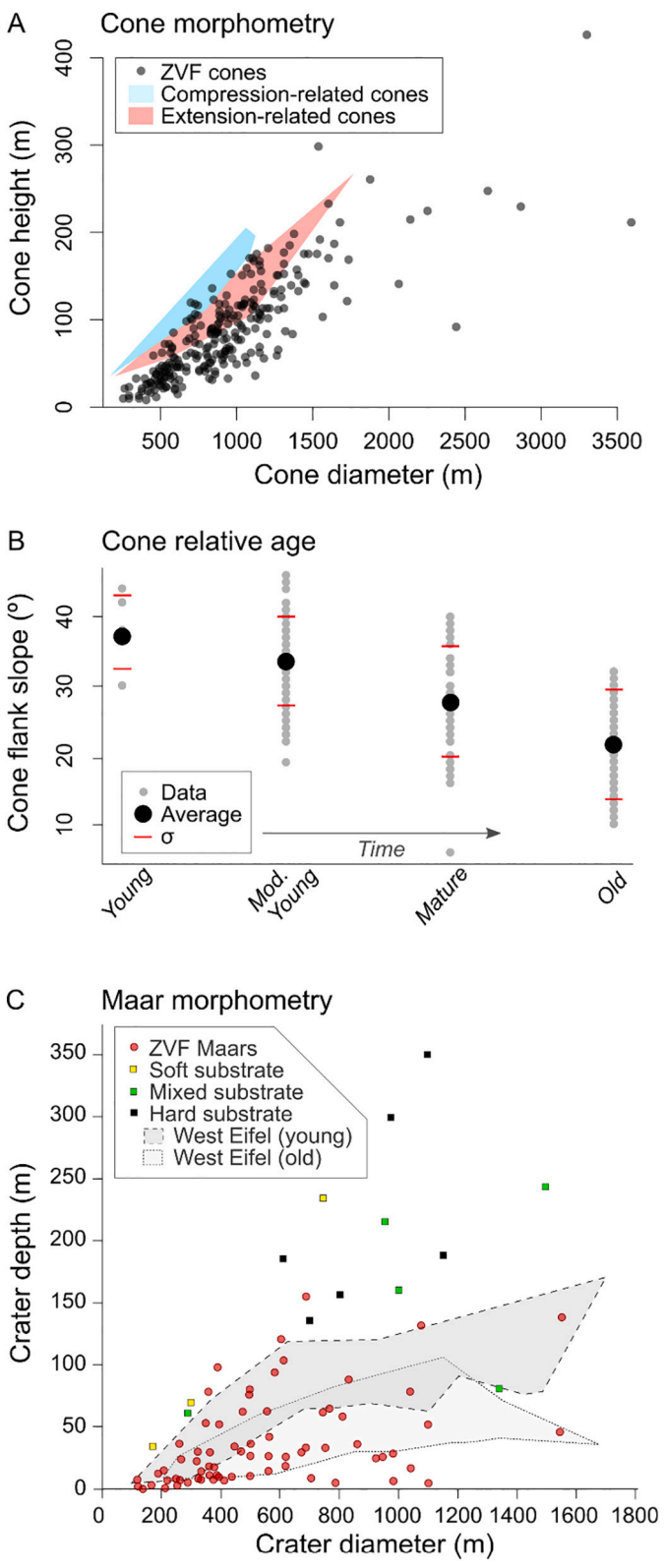

Fig. 12. Morphometric comparison of monogenetic landforms presents at ZVF: A) cinder cones morphometry, modified from Fornaciai et al. (2012); σ = standard deviation; B) relative age morphometry; C) maars morphometry and its relationship with substrate styles, modified from Ross et al. (2011).

(Cembrano and Lara, 2009) (Fig. 13). The E-W orientation is also in agreement with several structures that control the emplacement of lavas on the Copahue Volcano (Bonali et al., 2016).

Our data reveals that back-arc monogenetic vents seem to concentrate along secondary faults that diverge from the LOFZ (Fig. 13A), possibly because of the strong oblique component acting on the CSVZ. In transtensional environments, secondary structures can diverge from the master fault, forming imbricated fans of extensional fractures (Kim et al., 2003; Fig. 13B). To date, the occurrence of monogenetic volcanism associated with these structures has only been observed in the Wulanhada volcanic field, in Northern China, where a strike-slip dextral fault accommodates deformation and controls the distribution of monogenetic volcanoes (Zhao et al., 2019). In contrast, Wulanhada deposits are considerably smaller (in terms of area) when compared to the CSVZ, with only 41 vents and deposits that cover ~180 km^2 (Zhao et al., 2019).

Another important feature in the CSVZ is the Loncopué Trough (Rojas Vera et al., 2014; Pesce et al., 2019, 2020). Located between the main volcanic arc and the Agrio Fold and Thrust Belt, this 300 km long extensional structure controls the occurrence of monogenetic volcanism (Rojas Vera et al., 2014; Fig. 13A, C). Inside the Loncopué Trough, the monogenetic magmatism develops as continuous lava plateaus from early Pliocene to the present (Rojas Vera et al., 2014). Based on fieldwork and geophysical data, the Loncopué Trough seems to be associated with tearing of the subducted Nazca plate underneath the South American Plate, resulting in abnormal heat flow in the region (Rojas Vera et al., 2014). In this scenario, monogenetic activity seems to be controlled by the extensional regime at the Loncopué Trough, in addition to the oblique tectonics of the LOFZ.

In this setting, the growth and orientation of monogenetic volcanoes can be extensively controlled by transcurrent faults (e.g., Pasquare and Tibaldi, 2003; Tibaldi and Bonali, 2018; Tibaldi et al., 2017; Zhao et al., 2019). However, Pasquare and Tibaldi (2003) show that dykes are emplaced parallel to the regional σHmax, regardless of the volcano/fault proximity. This could explain why most monogenetic volcanoes in the ZVF present EN*E*-WNW trending basalt elongations and alignment, following the regional shortening induced by the Andean orogeny.

Monogenetic volcanoes in CSVZ also reveal changes in σHmax direction, which seem to be mainly controlled by their distance to the master LOFZ, or possibly by interference secondary structural features in the Loncopué Trough and the fold and thrust belt (Fig. 13A, B, C). The north end of the monogenetic field is marked by NE-SW-trending σHmax, almost parallel to σHmax observed in the main magmatic arc (Fig. 13A). This orientation is compatible with extensional faults and *horsetail splays* frequently observed at the end of strike-slip structures such as the LOFZ (Kim et al., 2003). The northern limit of the Loncopué Trough is marked by a significant change in the σHmax from NE-SW to the E-W (Fig. 13A). This σHmax E-W direction progressively rotates toward NE-SW was we move south in the Loncopué Trough (Fig. 13A). There is another significant change in the σHmax at ca. 38°30′, where σHmax becomes E-W oriented (Fig. 13A). Further south in the CSVZ, σHmax becomes less constrained and presents variable orientations, including NW-SE, NNW-SSE, and N-S (Fig. 13D).

Changes in the stress orientation using volcano morphology have been recently reported in the Java Volcanic Arc (Marliyani et al., 2020). The authors associated the progressive changes in σHmax to relative plate convergence and upper plate structure, while abrupt changes are linked to the presence of preexisting structures, as well as to interference of polygenetic volcanoes (Marliyani et al., 2020). Different from Java, monogenetic volcanoes in the CSVZ are predominantly located several kilometers away from the main volcanic arc (Fig. 1B). In this context, the only cluster expected to suffer influence from the arc is cluster 9, which presents a bimodal distribution of basal elongation (Fig. 9A, F).

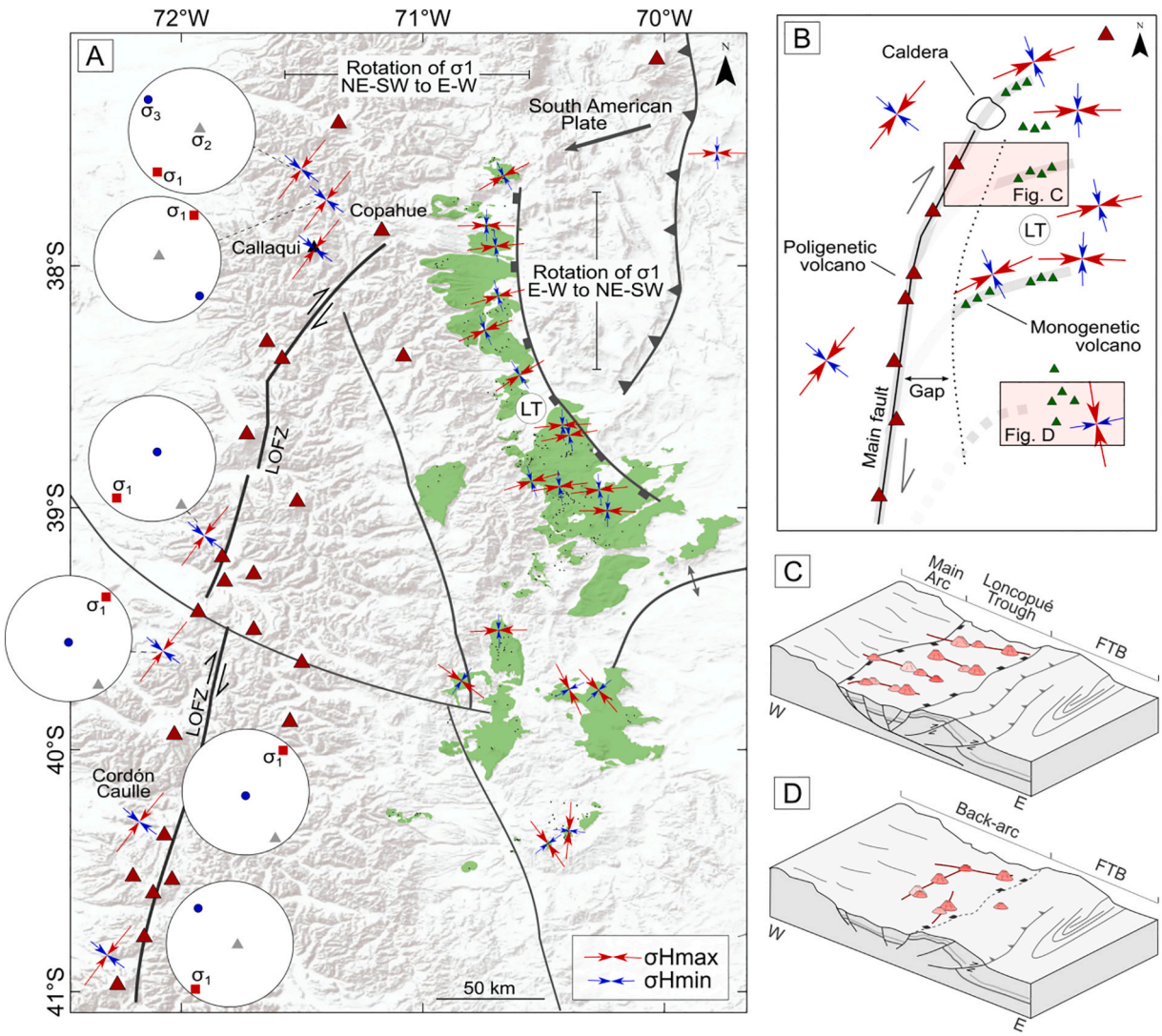

Fig. 13. Tectonic model for monogenetic volcanism in the CSVZ: A) regional map with main structural features, polygenetic volcanoes, and monogenetic deposits. B) Conceptual model for the emplacement of monogenetic volcanoes in the CSVZ; C) detail of the Loncopué Trough region next to cluster 5; D) detail of the southern CSVZ. Stereoplots indicate available data from the literature (Lara et al., 2006; Melnick and Echtler, 2006; Cembrano and Lara, 2009, Pardo et al., 2006; Lange et al., 2008; Potent and Reuther, 2001; Rosenau, 2004; Lavenu and Cembrano, 1999; Arancibia et al., 1999; Sielfeld et al., 2017). Legends are the same as Fig. 1. LT = Loncopué Trough, FTB = Fold and thrust belt.

5.4. *Timing and recurrence of monogenetic activity*

Absolute ages are scarce for ZVF and mainly concentrated at ~39°S. Most results indicate quaternary ages for the monogenetic activity, although the presence of multiple magmatic pulses is still unclear. Samples from the Loncopué Trough indicate ages between 2.30±0.3 and 0.47±0.2 Ma (K- Ar whole-rock; Linares and Gonzalez, 1990). Ages of 0.130±0.02, 0.167±0.005, 2.50±5, and 809±12 ka are also reported for basaltic lavas further along the same structure (^{40}Ar-^{39}Ar; Rabassa et al., 1987; Rojas Vera et al., 2014). Additional ages ranging from 1.6±0.2 and 0.9±0.3 Ma (K—Ar whole-rock) are also reported by Muñoz and Stern (1985, 1988) for samples in the Pino Hachado region, in the southernmost ZVF.

In this scenario of scarce absolute ages, relative age maps offer an alternative method for mapping the monogenetic activity through time (e.g., Haag et al., 2019). The interpolated relative age maps (Fig. 11) suggest a waning monogenetic activity in the ZVF over time: while the older monogenetic volcanoes are widespread in the ZVF (Fig. 11D), the younger landforms seem to be focused in the central segment of the volcanic field (Fig. 11A), near to the Zapala and Loncopué towns.

Geological mapping and fieldwork in the study area also suggest multiple episodes of monogenetic activity in the region (Rojas Vera et al., 2014; Pesce et al., 2019). Intercalated basaltic flows and glacial deposits are reported along the Loncopué trough (Folguera et al., 2003), suggesting at least two magmatic pulses in the region. Additional mapping by Báez et al. (2020) in the Caviahue-Copahue Volcanic Complex indicates the occurrence of at least two glaciations in the region (at 57–29 ka and/or 26.5–19.0 ka and at 14.5–11.9 ka). The 809 Ka basaltic flows are incised by a glacial valley in the western Loncopué Trough (Rojas Vera et al., 2014). These glacial valleys also control emplacement of younger, post-glacial activity with estimated ages to be less than 27 ka (Rojas Vera et al., 2014).

Monogenetic eruptions can be triggered by several factors because of their shallow magma storage generally in near-surface sills and dikes. Bonali et al. (2013) report stress changes induced by earthquakes in the SVZ. In the area, several earthquake-induced eruptions can occur as far as 500 km from their epicenters (Bonali et al., 2013). This finding highlights the role of earthquakes in inducing monogenetic activity, especially in subduction zones such as the SVZ (González et al., 2021).

The predominance of *E*-W and NE-SW feeding systems in the CSVZ is

at odds with the regime responsible for the development of the Loncopué Trough, which is mainly associated with N-S normal faults developed under E-W extension (Rojas Vera et al., 2014). This information suggests a decoupling between the stress state recorded by monogenetic feeding systems and the structural setting at the Loncopué Trough. Curiously, numerous N-S trending normal faults cut the monogenetic deposits to the east of Caviahue and next to the Loncopué Town (Rojas Vera et al., 2014; Pesce et al., 2019), suggesting ongoing deformation of the quaternary monogenetic volcanism.

5.5. Comparison with monogenetic fields in the Central Andes

For a long time, the study of monogenetic volcanoes has been hampered by the coarse resolution of DEMs and imagery data. Therefore, a greater focus has been placed on the study of large, polygenetic volcanoes. However, in recent years, the available high-resolution DEMs allowed the identification of thousands of monogenetic volcanoes in the Andean Cordillera.

Most of these studies have been focused in the Central Volcanic Zone of the Andes (CVZ; 18–28° S; e.g., Maro and Caffe, 2016; Tibaldi et al., 2017; Tibaldi and Bonali, 2018; Filipovich et al., 2019; Haag et al., 2019; Grosse et al., 2020; Morfulis et al., 2020; Ureta et al., 2021c). In contrast, studies involving geomorphologic characterization of monogenetic volcanoes in the Southern Volcanic Zone (SVZ) of the Andes are still scarce. In this section, we compare our results obtained at the ZVF (in the Central SVZ) with the available data for the CVZ (mainly for the southern Puna Plateau and northern Chile). A summary of this comparison is presented in Table 2.

Monogenetic volcanoes in the ZVF present a higher number of phreatomagmatic volcanoes (20%) when compared to other monogenetic fields in the Andes, such as the southern Puna Plateau (Haag et al., 2019) and northern Chile (Ureta et al., 2021c). This difference could be attributed to climate variations between these regions: while the ZVF is marked by a wet climate with the presence of lakes and vegetation, the CVZ sits above 3 km and comprises one of the aridest regions on Earth. The presence of sedimentary rocks of the Neuquén Basin as underlying units in the ZVF may also contribute to the occurrence of phreatomagmatism. In contrast, overlying units in the southern Puna Plateau are mainly metamorphic and igneous rocks (Schnurr et al, 2006; Seggiaro et al., 2006).

Another important fact to be considered is the absence of lava domes in the ZVF. Conversely, flat-topped and irregular lava domes are expressive and widespread monogenetic landforms in the southern Puna Plateau (Haag et al., 2019), as well as in the entire CVZ of the Andes (Ureta et al., 2021c). We interpret this absence of lava domes in the CSVZ as a result of contrasting melt compositions and evolution in these two areas. Magmas associated with the ZVF are mainly basalts with arc to back-arc signatures (Varekamp et al., 2010; Rojas Vera et al., 2014). In contrast, the monogenetic volcanism in southern Puna Plateau and northern Chile includes more evolved terms, such as basaltic-andesites and andesites.

In this scenario, the presence of lava domes may reflect contrasting petrogenetic conditions in the CVZ and SVZ: while the southern Puna is marked by crustal thickness of ~70 km (Trumbull et al., 2006), the ZVF crust is considerably thinner, ranging from 30 to 35 km (Munizaga et al., 1988; Nelson et al., 1993; Stern, 2004), yielding less evolved magmas and the absence of lava domes. This observation is also supported by petrogenetic models in northern Chile, where crustal thickness is also considerably higher than the SVZ (Yuan et al., 2002; Ureta et al., 2021c and references therein).

Table 2
Comparison of monogenetic volcanism in the SVZ and the CVZ of the Andes.

Parameters	Region of the Andes		
	South (Central SVZ at ZVF)	Central (Southern Puna Plateau)	Central (Northern Chile)
Edifice morphology	80% Cinder Cones 20% Pheatomagmatic 0% Domes	76% Cinder Cones 15% Domes 7% Pheatomagmatic (Haag et al., 2019)	35% Domes 33% Lava flows 30% Cinder Cones 2% Pheatomagmatic (Ureta et al., 2021c)
Cone diameter - Wco (m)	246 to 3590	200 to 3800 (Haag et al., 2019)	Not available
Cone height-Hco (m)	7 to 426	2 to 308 (Haag et al., 2019)	Not available
Average vent density (vents /km^2)	0.015	0.0083 (Haag et al., 2019)	0.0195 (Ureta et al., 2021c)
Maximum vent density (vents/km^2)	0.144	0.149 to 0.237 (Haag et al., 2019, Morfulis et al., 2020)	0.03 (Ureta et al., 2021c)
Exogenous controls – climate	Arid and wet	Predominately arid (Filipovich et al., 2019; Haag et al., 2019)	Predominately arid (Ureta et al., 2021c)
Subduction style and regional σ1	Oblique, NE-SW (Lara et al., 2006 and references therein)	Almost orthogonal, NW-SE (Marrett and Emerman, 1992)	Almost orthogonal, E-W (Tibaldi and Bonali, 2018)
Vent alignment	E-W to ENE-WSW (primary) and N-S (reactivated?)	NNE-SSW (reactivated); NW-SE (normal; strike-slip) (Haag et al., 2019; Grosse et al., 2020)	NW-SE, NNW-SSE and NNE-SSW (Ureta et al., 2021c)
Monogenetic magmatism	Waning	Waxing (Haag et al., 2019)	Waning (Ureta et al., 2021c)
Crustal thickness	30–35 km (Munizaga et al., 1988; Nelson et al., 1993; Stern, 2004)	~ 70 km (Trumbull et al., 2006)	~ 36 to 60 km (Yuan et al., 2002)
Geochemical origin	Arc to back-arc (Varekamp et al., 2010; Rojas Vera et al., 2014)	Lithospheric delamination (Kay and Mahlburg Kay, 1993) and foundering (Schoenbohm and Carrapa, 2015)	Several sources (Ureta et al., 2021c and references therein)
Age	2.3 Ma - Recent (Linares and Gonzalez, 1990; Rabassa et al., 1987; Muñoz and Stern, 1985, 1988)	9.0 Ma - Recent (Risse et al., 2008; Drew et al., 2009; Schoenbohm and Carrapa, 2015)	26 Ma - Recent (Ureta et al., 2021c and references therein)

6. Conclusions

In this work, we combine imagery and digital elevation models to map the occurrence of monogenetic volcanoes in the back-arc region of the Central Southern Volcanic Zone (CSVZ) of the Andes. The main conclusions are:

1. The CSVZ presents a predominance of cinder cones (80%) followed by a significant number of phreatomagmatic volcanoes (20%). This data implies the strombolian as the main eruption style but also reveals an important role of water and hydromagmatism in the eruption dynamics of monogenetic vents. The occurrence of phreatomagmatism is either associated with climate or geological controls (basement porosity and water availability).
2. Monogenetic volcanoes are grouped into nine clusters. The higher vent densities are observed in the center of the CSVZ to the south of the Loncopué Though. Each cluster is marked by contrasting vent distribution and organization that reflect the interplay of tectonics and magmatism (e.g., Báez et al., 2017; Morfulis et al., 2020).
3. Monogenetic vents show a clear association with local and regional lineaments, suggesting a strong structural control on the occurrence

of monogenetic deposits. The main controls on the distribution of monogenetic vents are the oblique tectonics of the Liquiñe-Ofqui Fault Zone and the extensional Loncopué Though.

4. Based on edifice morphology and distribution, monogenetic volcanoes are preferentially emplaced along NE- SW and E-W trending structures that reflect the stress state in the CSVZ (e.g., Le Corvec et al., 2013; Marliyani et al., 2020).
5. With scarce absolute ages for the region, relative age offers an alternative approach to map monogenetic activity over time. This data suggests a decrease in the aerial extend of monogenetic activity in the CSVZ.
6. When compared to monogenetic deposits in the Central Andes, the Southern Andes are defined by higher vent densities, a higher number of phreatomagmatic landforms, and the absence of lava domes (Haag et al., 2019; Ureta et al., 2021c). This likely reflects climate and crustal structure differences of these two regions.

Declaration of competing interest

The authors declare that all research meets the ethical guidelines, including adherence to the legal requirements. The authors also declare no conflict of interest.

Acknowledgments

This article is part of F.S·S. PhD's thesis at Geosciences Institute at Universidade Federal do Rio Grande do Sul, sponsored by the Conselho Nacional de Desenvolvimento Científico e Tecnológico of Brazil. F.S.S thanks Coordenação de Aperfeiçoamento de Pessoal de Nível Superior (CAPES, Brazil) for the financial support. Carlos A. Sommer thanks Conselho Nacional de Desenvolvimento Científico e Tecnológico (CNPq, Brazil) for the research grant and financial support (305036/2018-8, 406825/2018-6). The authors are grateful to reviews of Károly Németh and two anonymous reviewers who provided important suggestions to improvement of the manuscript.

Appendix A. Supplementary data

Supplementary data associated with this article can be found in the online version, at https://doi.org/10.1016/j.geomorph.2022.108130. These data include the Google map of the most important areas described in this article.

References

Arancibia, G., Cembrano, J., Lavenu, A., 1999. Transpresión dextral y partición de la deformación en la Zona de Falla Liquiñe- Ofqui, Aisén, Chile (44–45°S). Rev.Geol. Chile 26 (1), 3–22.

Báez, W., Carrasco Nuñez, G., Giordano, G., Viramonte, J.G., Chiodi, A., 2017. Polycyclic scoria cones of the Antofagasta de la Sierra basin, Southern Puna plateau, Argentina. Geol. Soc. Lond., Spec. Publ. 446, 311–336. https://doi.org/10.1144/sp446.3.

Báez, A.D., Báez, W., Caselli, A.T., Martini, M.A., Sommer, C.A., 2020. The glaciovolcanic evolution of the Copahue volcano, Andean Southern Volcanic Zone, Argentina-Chile. J. Volcanol. Geotherm. Res. 396, 106866 https://doi.org/10.1016/j.jvolgeores.2020.106866.

Bemis, K.G., Ferencz, M., 2017. Morphometric analysis of scoria cones: the potential for inferring process from shape. Geol.Soc.Lond. 446 (1), 61–100. https://doi.org/10.1144/SP446.9.

Bishop, M.A., 2007. Point pattern analysis of eruption points for the Mount Gambier volcanic sub-province: a quantitative geographical approach to the understanding of volcano distribution. Area 39, 230–241. https://doi.org/10.1111/j.1475-4762.2007.00729.x.

Bonali, F.L., Corazzato, C., Tibaldi, A., 2011. Identifying rift zones on volcanoes: an example from La Réunion island, Indian Ocean. Bull. Volcanol. https://doi.org/10.1007/s00445-010-0416-1.

Bonali, F.L., Tibaldi, A., Corazzato, C., Tormey, D.R., Lara, L.E., 2013. Quantifying the effect of large earthquakes in promoting eruptions due to stress changes on magma pathway: the Chile case. Tectonophysics. https://doi.org/10.1016/j.tecto.2012.10.025.

Bonali, F.L., Corazzato, C., Bellotti, F., Groppelli, G., 2016. Active tectonics and its interactions with Copahue Volcano. In: Active Volcanoes of the World. https://doi.org/10.1007/978-3-662-48005-2_2.

Bruno, B.C., 2004. Clustering within rootless cone groups on Iceland and Mars: effect of nonrandom processes. J. Geophys. Res. 109 https://doi.org/10.1029/2004je002273.

Bruno, B.C., Fagents, S.A., Hamilton, C.W., Burr, D.M., Baloga, S.M., 2006. Identification of volcanic rootless cones, ice mounds, and impact craters on Earth and Mars: using spatial distribution as a remote sensing tool. J. Geophys. Res. 111 https://doi.org/10.1029/2005je002510.

Cañón- Tapia, E., 2016. Reappraisal of the significance of volcanic fields. J. Volcanol. Geotherm. Res. 310, 26–38. https://doi.org/10.1016/j.jvolgeores.2015.11.010.

Carbone, O., Franzese, J., Limeres, M., Delpino, D., Martínez, 2011. In: El Ciclo Precuyano (Triásico Tardío- Jurásico Temprano) en la Cuenca Neuquina. Geología Y Recursos Naturales de la Provincia del Neuquén. Asociación Geológica Argentina, Buenos Aires, pp. 63–75.

Cebriá, J.M., Martiny, B.M., López-Ruiz, J., Morán-Zenteno, D.J., 2011. The Parícutin calc-alkaline lavas: new geochemical and petrogenetic modelling constraints on the crustal assimilation process. J. Volcanol. Geotherm. Res. https://doi.org/10.1016/j.jvolgeores.2010.11.011.

Cembrano, J., Lara, L., 2009. The link between volcanism and tectonics in the southern volcanic zone of the Chilean Andes: a review. Tectonophysics 471, 96–113. https://doi.org/10.1016/j.tecto.2009.02.038.

Cembrano, J., Hervé, F., Lavenu, A., 1996. The Liquiñe Ofqui fault zone: a long-lived intra-arc fault system in southern Chile. Tectonophysics 259, 55–66. https://doi.org/10.1016/0040-1951(95)00066-6.

Cordani, U.G., Ramos, V.A., Fraga, L.M., Cegarra, M., Delgado, I., de Souza, K.G., Gomes, F.E.M., Schobbenhaus, C., 2016. Tectonic Map of South America. Scale 1: 5000 000. 2nd Paris. CGMW- Servicio Geológico Minero Argetino (SEGEMAR).

D'Elia, L., Martí, J., Muravchik, M., Bilmes, A., Franzese, J.R., 2016. Impact of volcanism on the sedimentary record of the Neuquén rift basin, Argentina: towards a cause and effect model. Basin Res. 30, 311–335. https://doi.org/10.1111/bre.12222.

Di Traglia, F., Morelli, S., Casagli, N., Garduño- Monroy, V., 2014. Semi- automatic delimitation of volcanic edifice boundaries: validation and application to the cinder cones of the Tancitaro- Nueva Italia region (Michoacán- Guanajuato Volcanic Field, Mexico). Geomorphology 219, 152–160. https://doi.org/10.1016/j.geomorph.2014.05.002.

Drew, S.T., Ducea, M.N., Schoenbohm, L.M., 2009. Mafic volcanism on the Puna Plateau, NW Argentina: implications for lithospheric composition and evolution with an emphasis on lithospheric foundering. Lithosphere 1, 305–318. https://doi.org/10.1130/l54.1.

Filipovich, R., Báez, W., Bustos, E., Villagrán, A., Chiodi, A., Viramonte, J.G., 2019. <sb:contribution><sb:title>Eruptive styles related to the monogenetic mafic volcanism of Pasto Ventura region, Southern Puna,</sb:title></sb:contribution><sb:host><sb:issue><sb:series><sb:title>Argentina</sb:title></sb:series></sb:issue></sb:host>. Andean Geol. 46 (2), 300–335.

Folguera, A., Ramos, V.A., Melnick, D., 2003b. Recurrencia en el desarrollo de cuencas de intraarco, Cordillera Neuquina (37°30'). Rev. Asoc. Geol. Argent. 58, 3–19.

Folguera, A., Zapata, T., Ramos, V.A., 2006. Late Cenozoic extension and the evolution of the Neuquén Andes. In: Evolution of an Andean Margin: A Tectonic And Magmatic View From the Andes to the Neuquén Basin (35°-39°S Lat). Geological Society of America. https://doi.org/10.1130/2006.2407(12).

Folguera, A., Rojas Vera, E., Bottesi, G., Zamora Valcarce, G., Ramos, V.A., 2010. The Loncopué Trough: a Cenozoic basin produced by extension in the southern Central Andes. J. Geodyn. 49, 287–295. https://doi.org/10.1016/j.jog.2010.01.009.

Folguera, A., Spagnuolo, M., Vera, E.R., Litvak, V., Orts, D., Ramos, V., 2011. Magmatismo Neógeno y Cuarternario. In: Geología y Recursos Naturales De La Provincia de Neuquén: XVIII Congreso Geológico Argentino, pp. 275–286.

Fornaciai, A., Favalli, M., Karátson, D., Tarquini, S., Boschi, E., 2012. Morphometry of scoria cones, and their relation to geodynamic setting: a DEM-based analysis. J. Volcanol. Geotherm. Res. 217–218, 56–72. https://doi.org/10.1016/j.jvolgeores.2011.12.012.

Franzese, J.R., Spalletti, L.A., 2001. Late Triassic–early Jurassic continental extension in southwestern Gondwana: tectonic segmentation and pre-break-up rifting. J. S. Am. Earth Sci. 14, 257–270. https://doi.org/10.1016/s0895-9811(01)00029-3.

Franzese, J., Spalletti, L., Pérez, I.G., Macdonald, D., 2003. Tectonic and paleoenvironmental evolution of Mesozoic sedimentary basins along the Andean foothills of Argentina (32°–54°S). J. S. Am. Earth Sci. 16, 81–90. https://doi.org/10.1016/s0895-9811(03)00020-8.

Gianni, G.M., Dávila, F.M., Echaurren, A., Fennell, L., Tobal, J., Navarrete, C., Quezada, P., Folguera, A., Giménez, M., 2018. A geodynamic model linking Cretaceous orogeny, arc migration, foreland dynamic subsidence and marine ingression in southern South America. Earth Sci. Rev. 185, 437–462. https://doi.org/10.1016/j.earscirev.2018.06.016.

González, G., Fujita, E., Shibazaki, B., Hayashida, T., Chiodini, G., Lucchi, F., Yokoyama, I., Nemeth, K., Mora-Amador, R., Moya, A., Chigna, G., Martí, J., Rouwet, D., 2021. Increment in the volcanic unrest and number of eruptions after the 2012 large earthquakes sequence in Central America. Sci. Rep. https://doi.org/10.1038/s41598-021-01725-1.

Groeber, P., 1928. Traslado del vulcanismo de la falda oriental de la cordillera hacia la ladera occidental. An. Soc. Argent. Estud. Geogr. 3 (1), 210–218.

Grosse, P., Ochi Ramacciotti, M.L., Escalante Fochi, F., Guzmán, S., Orihashi, Y., Sumino, H., 2020. Geomorphology, morphometry, spatial distribution and ages of mafic monogenetic volcanoes of the Peinado and Incahuasi fields, southernmost Central Volcanic Zone of the Andes. J. Volcanol. Geotherm. Res. 401, 106966 https://doi.org/10.1016/j.jvolgeores.2020.106966.

Haag, M.B., Báez, W.A., Sommer, C.A., Arnosio, J.M., Filipovich, R.E., 2019. Geomorphology and spatial distribution of monogenetic volcanoes in the southern

Puna Plateau (NW Argentina). Geomorphology 342, 196–209. https://doi.org/10.1016/j.geomorph.2019.06.008.
Hasenaka, T.E., Carmichael, I.S.E., 1985. A compilation of location, size, and geomorpho-logical parameters of volcanoes of the Michoacan-Guanajuato volcanic field, central Mexico. Geofis.Int. 24, 577–607.
Hickey-Vargas, R., Sun, M., López-Escobar, L., Moreno-Roa, H., Reagan, M.K., Morris, J. D., Ryan, J.G., 2002. Multiple subduction components in the mantle wedge: evidence from eruptive centers in the Central Southern volcanic zone,Chile. Geology 30, 199. https://doi.org/10.1130/0091-7613(2002)030.
Hooper, D.M., Sheridan, M.F., 1998. Computer-simulation models of scoria cone degradation. J. Volcanol. Geotherm. Res. 83, 241–267. https://doi.org/10.1016/s0377-0273(98)00031-6.
Howell, J.A., Schwarz, E., Spalletti, L.A., Veiga, G.D., 2005. The Neuquén Basin: an overview. Geol. Soc. Lond., Spec. Publ. 252, 1–14. https://doi.org/10.1144/gsl.sp.2005.252.01.01.
Inbar, M., Gilichinsky, M., Melekestsev, I., Melnikov, D., Zaretskaya, N., 2011. Morphometric and morphological development of Holocene cinder cones: a field and remote sensing study in the Tolbachik volcanic field, Kamchatka. J. Volcanol. Geotherm. Res. 201, 301–311. https://doi.org/10.1016/j.jvolgeores.2010.07.013.
Kay, R.W., Mahlburg Kay, S., 1993. Delamination and delamination magmatism. Tectonophysics 219, 177–189. https://doi.org/10.1016/0040-1951(93)90295-u.
Kay, S.M., Ardolino, A.A., Gorring, M.L., Ramos, V.A., 2006. The Somuncura large igneous province in Patagonia: interaction of a transient mantle thermal anomaly with a subducting slab. J. Petrol. 48, 43–77. https://doi.org/10.1093/petrology/egl053.
Kereszturi, G., Németh, K., 2012. Monogenetic basaltic volcanoes: genetic classification, growth, geomorphology and degradation. In: Updates in Volcanology - New Advances in Understanding Volcanic Systems. InTech. https://doi.org/10.5772/51387.
Kereszturi, G., Németh, K., 2012b. Structural and morphometric irregularities of eroded Pliocene scoria cones at the Bakony-Balaton Highland Volcanic Field, Hungary. Geomorphology 136, 45–58. https://doi.org/10.1016/j.geomorph.2011.08.005.
Kervyn, M., Ernst, G.G.J., Carracedo, J.-C., Jacobs, P., 2012. Geomorphometric variability of "monogenetic" volcanic cones: evidence from Mauna Kea,Lanzarote and experimental cones. Geomorphology 136 (1), 59–75. https://doi.org/10.1016/j.geomorph.2011.04.009.
Kim, Y.-S., Peacock, D.C.P., Sanderson, D.J., 2003. Mesoscale strike-slip faults and damage zones at Marsalforn, Gozo Island, Malta. J. Struct. Geol. 25, 793–812. https://doi.org/10.1016/s0191-8141(02)00200-6.
Kiyosugi, K., Connor, C.B., Wetmore, P.H., Ferwerda, B.P., Germa, A.M., Connor, L.J., Hintz, A.R., 2012. Relationship between dike and volcanic conduit distribution in a highly eroded monogenetic volcanic field: San Rafael, Utah, USA. Geology 40, 695–698. https://doi.org/10.1130/g33074.1.
Lange, D., Cembrano, J., Rietbrock, A., Haberland, C., Dahm, T., Bataille, K., 2008. First seismic record for intra-arc strike-slip tectonics along the Liquiñe-Ofqui fault zone at the obliquely convergent plate margin of the southern Andes. Tectonophysics 455, 14–24. https://doi.org/10.1016/j.tecto.2008.04.014.
Lara, L.E., Lavenu, A., Cembrano, J., Rodríguez, C., 2006. Structural controls of volcanism in transversal chains: resheared faults and neotectonics in the Cordón Caulle-Puyehue area (40.5°S), Southern Andes. J. Volcanol. Geotherm. Res. 158, 70–86. https://doi.org/10.1016/j.jvolgeores.2006.04.017.
Lavenu, A., Cembrano, J., 1999. Compressional- and transpressional-stress pattern for Pliocene and Quaternary brittle deformation in fore arc and intra-arc zones (Andes of Central and Southern Chile). J. Struct. Geol. 21, 1669–1691. https://doi.org/10.1016/s0191-8141(99)00111-x.
Le Corvec, N., Spörli, K.B., Rowland, J., Lindsay, J., 2013. Spatial distribution and alignments of volcanic centers: clues to the formation of monogenetic volcanic fields. Earth Sci. Rev. 124, 96–114. https://doi.org/10.1016/j.earscirev.2013.05.005.
Leanza, H.A., Hugo, C.A., Herrero, J.C., Donnari, E.I., Pucci, J.C., 1997. Hoja geológica 3969- III Picun Leufú. Servicio Geológico Minero Argentino (SEGEMAR) Boletín N° 218, 135.
Lesti, C., Giordano, G., Salvini, F., Cas, R., 2008. Volcano tectonic setting of the intraplate, Pliocene-Holocene, Newer Volcanic Province (southeast Australia): role of crustal fracture zones. J. Geophys. Res. 113 https://doi.org/10.1029/2007jb005110.
Linares, E., Gonzalez, R.R., 1990. Catálogo de edades radimétricas de la República Argentina 1957-1987. Asociación Geológica Argentina, Publicaciones Especiales Série B, Didáctica y Complementaria, 19- 1- 628.
Marliyani, G.I., Helmi, H., Arrowsmith, J.R., Clarke, A., 2020. Volcano morphology as an indicator of stress orientation in the Java Volcanic Arc, Indonesia. J. Volcanol. Geotherm. Res. 400, 106912 https://doi.org/10.1016/j.jvolgeores.2020.106912.
Maro, G., Caffe, P.J., 2016. Neogene monogenetic volcanism from the Northern Puna region: products and eruptive styles. Geol. Soc. Lond., Spec. Publ. 446, 337–359. https://doi.org/10.1144/sp446.6.
Marrett, R., Emerman, S.H., 1992. The relations between faulting and mafic magmatism in the Altiplano-Puna plateau (central Andes). Earth Planet. Sci. Lett. 112, 53–59. https://doi.org/10.1016/0012-821x(92)90006-h.
Melnick, D., Echtler, H.P., 2006. Morphotectonic and geologic digital map compilations of the south-central Andes (36°–42°S). In: The Andes. Springer, Berlin Heidelberg, pp. 565–568. https://doi.org/10.1007/978-3-540-48684-8_30.
Morabito Garcia, E., Folguera, A., 2005. El alto de Copahue- Pino Hachado y la fosa de Loncopué: un comportamiento tectónico episódico, Andes neuquinos (37°- 39°S).
Morfulis, M., Báez, W., Retamoso, S., Bardelli, L., Filipovich, R., Sommer, C.A., 2020. Quantitative spatial distribution analysis of mafic monogenic volcanism in the southern Puna, Argentina: implications for magma production rates and structural control during its ascent. J. S. Am. Earth Sci. 104, 102852 https://doi.org/10.1016/j.jsames.2020.102852.
Mpodozis, C., Ramos, V.A., 2008. Tectónica jurásica en Argentina y Chile: extensión, subducción oblicua, rifting, deriva y colisiones. Rev. Asoc. Geol. Argent. 63 (4), 481–497.
Munizaga, F., Herve, F., Drake, R., Pankhurst, R.J., Brook, M., Snelling, N., 1988. Geochronology of the Lake Region of south-central Chile (39°–42°S): preliminary results. J. S. Am. Earth Sci. 1, 309–316. https://doi.org/10.1016/0895-9811(88)90009-0.
Muñoz, J., Stern, C., 1985. El complejo volcánico Pino Hachado en el sector nor-ccidental de la Patagonia (38°- 39°S): volcanismo plio- cuaternario trasarco en Sudamérica. IV° Congreso Geológico Chileno (Antofagasta). Actas 3, 381–412.
Muñoz, B.J., Stern, C.R., 1988. The quaternary volcanic belt of the southern continental margin of South America: transverse structural and petrochemical variations across the segment between 38°S and 39°S. J. S. Am. Earth Sci. 1, 147–161. https://doi.org/10.1016/0895-9811(88)90032-6.
Muñoz, J.B., Stern, C.R., 1989. Alkaline magmatism within the segment 38°-39°S of the Plio-Quaternary Volcanic Belt of the southern South American Continental Margin. J. Geophys. Res. 94, 4545–4560. https://doi.org/10.1029/jb094ib04p04545.
Nakamura, K., 1977. Volcanoes as possible indicators of tectonic stress orientation – principle and proposal. J. Volcanol. Geotherm. Res. 2, 1–16.
Nelson, E., Forsythe, R., Diemer, J., Allen, M., Urbina, O., 1993. Taitao ophiolite: a ridge collision ophiolite in the forearc of the southern Chile (46° S). Rev.Geol.Chile 20 (2), 137–165.
Németh, K., Kereszturi, G., 2015. Monogenetic volcanism: personal views and discussion. Int. J. Earth Sci. 104, 2131–2146. https://doi.org/10.1007/s00531-015-1243-6.
Pardo, M., Vera, E., Monfret, T., Yánez, G., Eisenber, A., 2006. Sismicidad cortical superficial bajo Santiago: implicaciones en la tectónica andina y evaluación del pelidro sísmico. In: Actas XI Congreso Geológico Chileno, 1, pp. 443–446.
Pasquare, F.A., Tibaldi, A., 2003. Do transcurrent faults guide volcano growth? The case of NW Bicol Volcanic Arc, Luzon, Philippines. Terra Nova. https://doi.org/10.1046/j.1365-3121.2003.00484.x.
Paulsen, T.S., Wilson, T.J., 2010. New criteria for systematic mapping and reliability assessment of monogenetic volcanic vent alignments and elongate volcanic vents for crustal stress analyses. Tectonophysics 482, 16–28. https://doi.org/10.1016/j.tecto.2009.08.025.
Pérez-López, R., Legrand, D., Garduño-Monroy, V.H., Rodríguez-Pascua, M.A., Giner-Robles, J.L., 2011. Scaling laws of the size-distribution of monogenetic volcanoes within the Michoacán-Guanajuato Volcanic Field (Mexico). J. Volcanol. Geotherm. Res. 201, 65–72. https://doi.org/10.1016/j.jvolgeores.2010.09.006ps.
Pesce, A., Gimenez, M.E., Gianni, G.M., Folguera, A., Martinez, P., 2019. Magnetic characterization of a retroarc extensional basin: the Loncopué Trough. J. S. Am. Earth Sci. 89, 55–62. https://doi.org/10.1016/j.jsames.2018.11.001.
Pesce, A., Gimenez, M.E., Castiglione, B., Gianni, G.M., Folguera, A., 2020. Sección eléctrica cortical a través de la Fosa de Loncopué. Rev. Asoc. Geol. Argent. 78 (2), 333–337.
Potent, S., Reuther, C.D., 2001. In: Neogene Deformationsprozesse im Aktiven magmatischen Bogen SudCentralChiles zwichen 37° und 39°S, 85. Mitteilungen aus dem Geologisch- PaleoÉontologischen Institut der UniversitaÉt Hamburg, pp. 1–2.
Rabassa, J., Everson, E., Schlieder, G., Clinch, J.M., Stephens, G., Zeitler, P., 1987. Edad Pre- Pleistoceno superior de la glaciación El Cóndor, Valle del Río Malleo, Neuquén. 10° Congreso Geológico Argentino (Tucumán). Actas 4, 217–219.
Radic, J.P., Rojass, L., Carpinelli, A., Zurita, E., 2002. Evolución tectónica de la cuenca terciaria de Cura- Mallín, región cordillerana chilena Argentina (36 30'- 39 00"S). In: Congreso Geológico Argentino, 15, pp. 233–241.
Ramos, V.A., Folguera, A., 2005. Tectonic evolution of the Andes of Neuquén: constraints derived from the magmatic arc and foreland deformation. Geol. Soc. Lond., Spec. Publ. 252, 15–35. https://doi.org/10.1144/gsl.sp.2005.252.01.02.
Risse, A., Trumbull, R.B., Coira, B., Kay, S.M., van den Bogaard, P., 2008. 40Ar/39Ar geochronology of mafic volcanism in the back-arc region of the southern Puna plateau, Argentina. J. S. Am. Earth Sci. 26, 1–15. https://doi.org/10.1016/j.jsames.2008.03.002.
Rojas Vera, E.A., Folguera, A., Valcarce, G.Z., Giménez, M., Ruiz, F., Martínez, P., Bottesi, G., Ramos, V.A., 2010. Neogene to Quaternary extensional reactivation of a fold and thrust belt: the Agrio belt in the Southern Central Andes and its relation to the Loncopué trough (38°–39°S). Tectonophysics 492, 279–294. https://doi.org/10.1016/j.tecto.2010.06.019.
Rojas Vera, E.A., Sellés, D., Folguera, A., Gímenez, M., Ruíz, F., Orts, D., Zamora Valcarce, G., Martínez, P., Bechis, F., Ramos, V.A., 2014. The origin of the Loncopué Trough in the retroarc of the Southern Central Andes from field, geophysical and geochemical data. Tectonophysics 637, 1–19. https://doi.org/10.1016/j.tecto.2014.09.012.
Rosenau, M.R., 2004. Tectonics of the Southern Andean Intra-arc Zone (38° - 42°S). Freie Universität, Berlin. https://doi.org/10.17169/REFUBIUM-6146.
Ross, P.-S., Delpit, S., Haller, M.J., Németh, K., Corbella, H., 2011. Influence of the substrate on maar–diatreme volcanoes — an example of a mixed setting from the Pali Aike volcanic field, Argentina. J. Volcanol. Geotherm. Res. 201, 253–271. https://doi.org/10.1016/j.jvolgeores.2010.07.018.
Schnurrel al., n.d. W.B.W. Schnurr A. Risse R.B. Trumbull K. Munier , n.d. Digital Geological Map of the Southern and Central Puna Plateau, NW Argentina, in: The Andes. Springer Berlin Heidelberg, pp. 563–564. doi:10.1007/978-3-540-48684-8_29.
Schoenbohm, L.M., Carrapa, B., 2015. Miocene–Pliocene shortening, extension, and mafic magmatism support small-scale lithospheric foundering in the central Andes, NW Argentina. In: Geodynamics of a Cordilleran Orogenic System: The Central

Andes of Argentina And Northern Chile. Geological Society of America. https://doi.org/10.1130/2015.1212(09).
Seggiaro, R., Hongn, F., Folguera, A., Clavero, J., 2006. Hoja Geológica 2769-II. In: Boletín, 294. Instituto de Geología y Recursos Minerales, Servicio Geológico Minero Argentino, Paso de San Francisco.
Sielfeld, G., Cembrano, J., Lara, L., 2017. Transtension driving volcano-edifice anatomy: insights from Andean transverse-to-the-orogen tectonic domains. Quat. Int. 438, 33–49. https://doi.org/10.1016/j.quaint.2016.01.002.
Smith, I.E.M., Németh, K., 2017. Source to surface model of monogenetic volcanism: a critical review. Geol. Soc. Lond., Spec. Publ. 446, 1–28. https://doi.org/10.1144/sp446.14.
Sonder, I., Harp, A.G., Graettinger, A.H., Moitra, P., Valentine, G.A., Büttner, R., Zimanowski, B., 2018. Meter-scale experiments on magma-water interaction. J. Geophys. Res. Solid Earth 123. https://doi.org/10.1029/2018jb015682.
Stern, C.R., 2004. Active Andean volcanism: its geologic and tectonic setting. Rev.Geol. Chile 31. https://doi.org/10.4067/s0716-02082004000200001.
Tadini, A., Bonali, F.L., Corazzato, C., Cortés, J.A., Tibaldi, A., Valentine, G.A., 2014. Spatial distribution and structural analysis of vents in the Lunar Crater Volcanic Field (Nevada, USA). Bull. Volcanol. https://doi.org/10.1007/s00445-014-0877-8.
Tibaldi, A., 1995. Morphology of pyroclastic cones and tectonics. J.Geophys.Res. 100, 24521–24535. https://doi.org/10.1029/95jb02250.
Tibaldi, A., Bonali, F.L., 2018. Contemporary recent extension and compression in the central Andes. J. Struct. Geol. https://doi.org/10.1016/j.jsg.2017.12.004.
Tibaldi, A., Bonali, F.L., Corazzato, C., 2017. Structural control on volcanoes and magma paths from local- to orogen-scale: the central Andes case. Tectonophysics. https://doi.org/10.1016/j.tecto.2017.01.005.
Trumbullet al., n.d.Trumbull, R.B., Riller, U., Oncken, O., Scheuber, E., Munier, K., Hongn, F., n.d. The Time-Space Distribution of Cenozoic Volcanism in the South-Central Andes: a New Data Compilation and Some Tectonic Implications, in: The Andes. Springer Berlin Heidelberg, pp. 29–43. doi:10.1007/978-3-540-48684-8_2.
Tunik, M., Folguera, A., Naipauer, M., Pimentel, M., Ramos, V.A., 2010. Early uplift and orogenic deformation in the Neuquén Basin: constraints on the Andean uplift from U-Pb and Hf isotopic data of detrital zircons. Tectonophysics 489, 258–273. https://doi.org/10.1016/j.tecto.2010.04.017.
Ureta, G., Németh, K., Aguilera, F., Kósik, S., González, R., Menzies, A., González, C., James, D., 2021a. Evolution of a magmatic to a phreatomagmatic volcanic system: the birth of a monogenetic volcanic field, Tilocálar volcanoes, northern Chile. J. Volcanol. Geotherm. Res. https://doi.org/10.1016/j.jvolgeores.2021.107243.
Ureta, G., Németh, K., Aguilera, F., Zimmer, M., Menzies, A., 2021b. A window on mantle-derived magmas within the Central Andes: eruption style transitions at Cerro Overo maar and La Albóndiga lava dome, northern Chile. Bull. Volcanol. https://doi.org/10.1007/s00445-021-01446-3.
Ureta, G., Németh, K., Aguilera, F., Vilches, M., Aguilera, M., Torres, I., Pablo Sepúlveda, J., Scheinost, A., González, R., 2021. An overview of the Mafic and Felsic monogenetic Neogene to Quaternary volcanism in the Central Andes, Northern Chile (18-28°Lat.S). In: Németh, K. (Ed.), Updates in Volcanology - Transdisciplinary Nature of Volcano Science. IntechOpen, pp. 249–276. https://doi.org/10.5772/intechopen.93959. Available from: https://www.intechopen.com/chapters/74390.
Uslular, G., Gençalioğlu-Kuşcu, G., Arcasoy, A., 2015. Size-distribution of scoria cones within the Eğrikuyu Monogenetic Field (Central Anatolia, Turkey). J. Volcanol. Geotherm. Res. 301, 56–65. https://doi.org/10.1016/j.jvolgeores.2015.05.006.
Uslular, G., Le Corvec, N., Mazzarini, F., Legrand, D., Gençalioğlu-Kuşcu, G., 2021. Morphological and multivariate statistical analysis of quaternary monogenetic vents in the Central Anatolian Volcanic Province (Turkey): implications for the volcano-tectonic evolution. J. Volcanol. Geotherm. Res. 416, 107280 https://doi.org/10.1016/j.jvolgeores.2021.107280.
Varekamp, J.C., Hesse, A., Mandeville, C.W., 2010. Back-arc basalts from the Loncopue graben (Province of Neuquen, Argentina). J. Volcanol. Geotherm. Res. 197, 313–328. https://doi.org/10.1016/j.jvolgeores.2010.04.003.
Vergani, G.D., Tankard, A.J., Belotti, H.J., Welsink, H.J., 1995. Tectonic evolution and paleogeography of the Neuquén Basin, Argentina. AAPG Mem. 62, 383–402.
Vergara, M., Muñoz, J., 1982. La Formación Cola de Zorro en la alta cordillera Andina Chilena (36–39 Lat. S), sus características petrográficas y petrológicas: Una revisión. Rev.Geol.Chile 17 (1), 31–46.
Wood, C.A., 1979. Monogenetic volcanoes of the terrestrial planets. In: Proceedings of the 10th Lunar and Planetary Science Conference, Houston, Texas, March 19–23, 1979. Pergamon Press, Inc., New York, pp. 2815–2840.
Yuan, X., Sobolev, S.V., Kind, R., 2002. Moho topography in the central Andes and its geodynamic implications. Earth Planet. Sci. Lett. https://doi.org/10.1016/s0012-821x(02)00589-7.
Zannettini, J.C.M., Leanza, H.A., Giusiano, A., Santamaría, G.R., Franchi, M., 2010. Hoja Geológica 3972- II Loncopué. Servicio Geológico Minero Argentino (SEGEMAR) Boletin N° 381, 93.
Zarazúa-Carbajal, M.C., De la Cruz-Reyna, S., 2020. Morpho-chronology of monogenetic scoria cones from their level contour curves. Applications to the Chichinautzin monogenetic field, Central Mexico. J. Volcanol. Geotherm. Res. 407, 107093 https://doi.org/10.1016/j.jvolgeores.2020.107093.
Zhao, Y.-W., Fan, Q.-C., Zou, H.-B., Li, N., 2019. Tectonic controls of Late Cenozoic monogenetic intraplate volcanism at the Wulanhada volcanic field, Northern China. J. Volcanol. Geotherm. Res. 383, 16–27. https://doi.org/10.1016/j.jvolgeores.2018.01.022.